NATIONAL ADVISORY COMMITTEE FOR AERONAUTICS

TECHNICAL NOTE 2737

PLASTIC STRESS-STRAIN RELATIONS FOR COMBINED TENSION AND COMPRESSION

By Joseph Marin and H. A. B. Wiseman

The Pennsylvania State College

Washington
July 1952

NATIONAL ADVISORY COMMITTEE FOR AERONAUTICS

TECHNICAL NOTE 2737

PLASTIC STRESS-STRAIN RELATIONS FOR COMBINED TENSION AND COMPRESSION

By Joseph Marin and H. A. B. Wiseman

SUMMARY

The main purpose of this investigation was to determine the validity of the plasticity theories and the correctness of various assumptions made in these theories. For this purpose, plastic stress-strain relations for biaxial tension-compression principal stresses were determined for a 14S-T4 aluminum alloy. The combined tension and compression principal stresses were produced by subjecting a thin-walled tubular specimen to axial tension and torque.

To provide control data and information on the influence of biaxial stresses on strength, the usual constant-stress-ratio tests were made. These tests showed that the biaxial yield strength agrees best with the distortion-energy theory. Ductility and fracture strengths could not be determined because failure was produced in most cases by buckling. These constant-stress-ratio tests, covering principal stress ratios from 0 to -1.0, showed that the plastic stress-strain relations agree approximately with both the deformation and the flow theories.

Since the constant-stress-ratio tests cannot distinguish between the flow and deformation theories, variable-stress-ratio tests and special biaxial tests were conducted.

In a second type of test, the axial tensile load was first applied to the tubular specimen so as to produce a selected plastic strain value. The torque load was then applied to the specimen, thereby producing a variable principal stress ratio with increase in torque load. Tests were also made in which the torque load was first applied followed by the axial tensile load. The results of these variable-stress-ratio tests do not agree with either the flow or the deformation theories. However, for two tests with different paths of loading but the same final state of stress, the resultant strains were not the same. This difference in strain lends support to the flow rather than the deformation theory, since the latter theory requires that these strains be equal.

In a third type of test, tensile stress was first applied in the axial direction to specified strain values. The tensile stress was then completely removed and torsional stress was then applied. Tests were also conducted with the torsional stress first applied followed by the axial tensile stresses. This group of tests showed that the assumption of "isotropic strain-hardening" is not valid.

A fourth type of test was made to check the validity of the assumption that the directions of principal shear stresses and principal shear strains coincide. This check was made by measuring the principal strain directions by the use of strain rosettes and comparing these directions with the directions of the principal stresses during a loading condition with variable stress ratio. These tests indicate that the principal stress and strain directions do not coincide but that the strains in the directions of the principal stress are within about 2.5 percent of the principal strain values.

INTRODUCTION

Most combined plastic stress-strain relations have been determined for conditions in which the principal stress ratio remains constant in a test. Such tests cannot be used to determine which theory is the most suitable. Furthermore, constant-stress-ratio tests cannot be used to determine the validity of the assumptions made in the various theories. They do not distinguish between deformation- and flow-type theories.[1] The tests in this investigation were made in an attempt to fill these needs.

The research described in this report was performed in the Plasticity Laboratory of The Pennsylvania State College under the sponsorship and with the financial assistance of the National Advisory Committee for Aeronautics. Dr. S. B. Batdorf and his associates at the Langley Aeronautical Laboratory gave many helpful suggestions in the planning of this research program. Messrs. H. A. B. Wiseman, L. W. Hu, Yoh-Han Pao, and W. P. Hughes, research assistants, conducted the tests. Mr. H. A. B. Wiseman also computed the data and plotted the graphs. The testing machine, special strain gage, and specimens were made by Messrs. S. S. Eckley, L. H. Johnson, and I. Bjalme. The assistance given by the NACA and the foregoing individuals in making possible this investigation is greatly appreciated.

---

[1] When reference is made to the flow and deformation theories, the simple theories based on the octahedral shear stress and strain are intended.

SYMBOLS

D	plasticity modulus, psi
d	original internal diameter of tubular specimen, inches
E	Young's modulus of elasticity, psi
e_x	nominal axial strain, inches per inch
e_y	nominal radial strain, inches per inch
e_1, e_2	maximum and minimum principal strains, respectively, inches per inch
e_{1e}, e_{2e}	elastic maximum and minimum principal strains, respectively, inches per inch
L	gage length at any time, inches
L_o	original gage length, inches
M_t	torque load, inch-pounds
P	axial tension load, pounds
t	original wall thickness of tubular specimen, inches
x, y	principal stress ratios
α	principal strain direction
γ_{xy}	true shear strain, inches per inch
γ_{xy}'	nominal shear strain, inches per inch
γ_{xy_p}	true plastic shear strain, inches per inch
δ_{1x}, δ_{2x}	measured axial strains, inches per inch
$\bar{\epsilon}$	significant strain, inches per inch
ϵ_x	true axial strain, inches per inch
ϵ_{x_p}	true plastic axial strain, inches per inch

θ	principal stress direction
ρ	angle of twist in 2-inch gage length, degrees
σ	true stress in simple tension, psi
$\overline{\sigma}$	significant stress, psi
σ_x	true axial stress, psi
σ_x'	nominal axial stress, psi
σ_y	yield stress in simple tension
σ_1, σ_2	maximum and minimum principal stress, respectively, psi
σ_{1e}, σ_{2e}	elastic maximum and minimum principal stresses, respectively, psi
σ_{1y}, σ_{2y}	maximum and minimum yield principal stresses, respectively, psi
τ_{xy}	true shear stress, psi
τ_{xy}'	nominal shear stress, psi

TEST PROCEDURE

Material Tested and Specimens

The material tested was an aluminum alloy designated as 14S-T4. The material was supplied in the form of hot-rolled machined cylinders, $7\frac{1}{4}$ inches long with a $1\frac{5}{8}$-inch outside diameter and an 11/16-inch bore. The normal composition, in addition to aluminum and normal impurities, consists of 4.4 percent copper, 0.8 percent silicon, 0.8 percent manganese, and 0.4 percent magnesium. The Research Laboratories of the Aluminum Company of America supplied control data on the yield strength, tensile strength, and ductility. These data were obtained primarily to provide information on the degrees of anisotropy of the specimens. For this purpose, specimens taken from the cylinders were tested in the axial, lateral, and diagonal directions. The average values of the properties were: Yield strength, 36,300 psi ± 10.4 percent; tensile strength, 61,500 psi ± 2.8 percent; and elongation in 4 diameters, 21.4 percent ± 4.5 percent. The data supplied showed that only about

one-half the percentage variations in strength were due to anisotropy, the remaining differences being due to normal variations in the materials.

The dimensions of the machined specimen are given in figure 1. Both the inside and outside surfaces of the specimens were machined. The wall thickness of the tubular specimens was measured using the apparatus described in reference 1. The ratio of the wall thickness to diameter was selected so as to delay buckling as much as possible and at the same time to yield an essentially uniform stress distribution throughout the wall.

Testing Machine

The special tension-torsion machine, as shown in figure 2, was rebuilt to conduct the tests described in this report. The axial tensile load is applied to the tubular specimen S by means of the hydraulic jack H through the pulling rod R. The axial load is measured by the dynamometer D_a using SR-4 gages. The twisting moment is applied by a 3/4-horsepower, direct-current motor M and speed reducer SR. Variation in rate of application of torque load is provided by a rheostat RH and a motor-generator set. A disk D is attached to the lower part of the specimen to which cables C are connected passing over frictionless pulleys to the bar B. The torque is measured by the calibrated bar B using SR-4 strain-gage readings as indicated. A 2000-pound dial-type dynamometer D_t is attached to the bar B to check the foregoing torque value.

The SR-4 indicators I and switching unit SW for measuring the loads and elastic strains are shown in figure 3.

Method of Measuring Strains

A special mechanical-type strain gage was designed for the measurements of plastic angles of twist and axial strains as shown in figure 4. Attempts were made to develop a self-recording induction type of strain gage for measuring angles of twist and axial strains. This latter-type gage was abandoned since it could not be made to give reproducible results. By the mechanical gage in figure 4, axial strains were measured for a 2-inch gage length by the two 0.0001-inch dials placed 180° apart (fig. 4). The angles of twist were measured for a 2-inch gage length by the twistmeter part of the gage shown in figure 4. Attachment of the strain gage to the specimen during plastic flow was maintained by rods which bear on the specimen at one end and are connected by preloaded springs to the strain gage at the other end. By adequate initial spring pressure, the gage remained attached to the specimen without slipping even in cases where the specimen had considerable reduction in diameter.

Method of Testing

The specimen is first assembled in the testing machine with the elastic SR-4 gages and the special mechanical gage as shown in figure 4. Increments of axial tensile load and torque are then applied as prescribed by the particular test. For each load increment applied, axial-strain and angle-of-twist readings are recorded.

CONSTANT-STRESS-RATIO TESTS

Plastic stress-strain relations for various constant values of the biaxial stress ratios were obtained to provide information on the influence of biaxial stresses on the plastic stress-strain relations and on the yield strength.

Conventional Stress-Strain Results

The average conventional stress-strain curves for various principal stress ratios and for the axial and shear stress components are shown in figures 5(a) and 5(b). The values of the nominal axial and average shear stresses used in figure 5 were respectively determined by

$$\sigma_x' = \frac{P}{\pi t(d + t)} \tag{1}$$

and

$$\tau_{xy}' = \frac{2M_t}{\pi t(d + t)^2} \approx \frac{2M_t}{\pi dt(d + 2t)} \tag{2}$$

where

P	axial load
M_t	twisting moment
d	internal diameter of specimen
t	wall thickness

The nominal axial and shear strains for the above stresses, in terms of the measured strains are, respectively,

$$e_x = \frac{\delta_{1x} + \delta_{2x}}{2L_o} \tag{3}$$

$$\gamma_{xy}' = \frac{\pi}{360} \frac{(d + t)\rho}{L_o} \tag{4}$$

where

δ_{1x}, δ_{2x} measured axial elongations on opposite sides of specimens

L_o gage length

ρ angle of twist, degrees

The shear strain at the center line of the tube wall is used in defining the shear strain in equation (4), since this measure of strain is consistent with using the average shear stress defined by equation (2).

The initial elastic part of the nominal stress-strain diagrams is shown in figures 6(a) and 6(b) for the maximum and minimum nominal principal stress values. The values of the nominal principal stresses and strains used for plotting figures 6(a) and 6(b) have been shown to be, respectively,

$$\left.\begin{matrix}\sigma_{1e} \\ \sigma_{2e}\end{matrix}\right\} = \frac{\sigma_x'}{2} \pm \sqrt{\left(\frac{\sigma_x'}{2}\right)^2 + (\tau_{xy}')^2} \tag{5}$$

$$\left.\begin{matrix}e_{1e} \\ e_{2e}\end{matrix}\right\} = \frac{e_x + e_y}{2} \pm \frac{1}{2}\sqrt{(e_x - e_y)^2 + (\gamma_{xy}')^2} \tag{6}$$

To define elastic failure or yielding, the yield strength in simple tension will be determined based on an offset strain of 0.002 inch per inch as shown in figure 6. For combined stresses an equivalent offset strain value was used to determine yielding as defined in reference 2. Values of these biaxial yield strengths (based on fig. 6) are shown in table 1 for various stress ratios.

Plastic Stress-Strain Results

To determine the plastic stress-strain relations, the changes in the dimensions of the specimens must be considered and the true stresses and strains calculated. Figures 7(a) and 7(b) give the average true plastic stress-strain relations considering the change in gage length and dimensions in the plastic range. The values of the true stress components in terms of the nominal stresses can be shown to be (reference 3), respectively,

$$\sigma_x = \sigma_x'\left(1 + e_x\right) \tag{7}$$

$$\tau_{xy} = \tau_{xy}'\left(1 + e_x\right)^{3/2} \tag{8}$$

Reference 3 also shows that the true strain components ϵ_x, in terms of the nominal strain e_x, is

$$\epsilon_x = \log_e\left(1 + e_x\right) \tag{9}$$

The true shear strain by equation (4) is $\gamma_{xy} = \pi\int(d + t)/(360L)$. Then if $d + t$ is assumed to remain constant, $\gamma_{xy}/\gamma_{xy}' = L_o/L$ or

$$\gamma_{xy} = \frac{\gamma_{xy}'}{1 + e_x} \tag{10}$$

The assumptions used in obtaining equation (10) lead to errors which are within experimental errors. The true stresses and strains used in plotting figure 7 are those defined in equations (7) to (10).

Analysis and Discussion

A comparison of the experimental and theoretical values of the yield strength for various biaxial stress ratios is given in figure 8. The theories shown in figure 8 include the distortion-energy and shear theories. A third theory by Prager (reference 4) was considered but was not included in this report since the theory is semiempirical. A comparison of the theoretical values and the test results shows that the yield strengths can be defined better by the distortion-energy theory than by the shear theory. The influence of combined stresses on the fracture and ultimate strengths could not be determined since most of the specimens failed by buckling. In all the test results given in this report, failure by buckling occurred unless otherwise stated. A

comparison of the deformation theory and experimental results was made by plotting the significant stress-strain relations (reference 5), where the significant stress and strain are, respectively,

$$\bar{\sigma} = \sqrt{(\sigma_x)^2 + 3\tau_{xy}^2} \tag{11}$$

$$\bar{\epsilon} = \sqrt{\left(\epsilon_{x_p}\right)^2 + \frac{1}{3}\left(\gamma_{xy_p}\right)^2} \tag{12}$$

It should be noted that equation (12) gives an approximate value for the significant strain, since it is assumed in equation (12) that the plastic strains are relatively small. Values of the strain components used in calculating the significant strain are the plastic strains or the total strains less the elastic strains. Figure 9 gives the significant stress-strain relations for various principal stress ratios. By the deformation theory and also by the flow theory all these relations should coincide with the simple-tension plastic stress-strain relation. An examination of figure 9 shows that the relations agree approximately and that the deformation or flow theories are, therefore, good approximations for defining the significant stress-strain relations for constant stress ratios. In figure 7 the plastic stress-strain relations are compared with the values predicted by the deformation theory. It should be recalled that for constant stress ratios the flow theory and deformation theory are identical. Figure 7 shows that the deformation theory gives a reasonable approximation to the test results.

In plotting the theoretical stress and strain values in figure 7 the following procedure is used. It is first noted that by the deformation theory the plastic strain components can be shown to be (reference 5)

$$\epsilon_{x_p} = \frac{1}{D}\left(\sigma_x - \frac{1}{2}\sigma_y - \frac{1}{2}\sigma_z\right) = \frac{\sigma_x}{D} \tag{13}$$

and

$$\gamma_{xy_p} = \frac{3}{D}\tau_{xy} \tag{14}$$

where D is the plasticity modulus. The total strains in terms of the stress components then become

$$\epsilon_x = \frac{\sigma_x}{E} + \frac{\sigma_x}{D} \tag{15}$$

and

$$\gamma_{xy} = \frac{2(1 + \mu)\tau_{xy}}{E} + \frac{3}{D}\tau_{xy} \tag{16}$$

From equations (11) and (12) for simple tension $\bar{\sigma}/\bar{\epsilon} = \sigma/\epsilon_p$ and by equation (13) for simple tension $\sigma/\epsilon_p = D$, or

$$\bar{\sigma}/\bar{\epsilon} = D \tag{17}$$

Equations (11), (13), (14), and (17) can now be used to find the theoretical stress-strain relations. For given values of σ_x and τ_{xy}, $\bar{\sigma}$ can be found by equation (11). Using the simple-tension plastic stress-strain relation in figure 9 for a given stress $\bar{\sigma}$ the strain $\bar{\epsilon}$ can be found from the curve and $D = \bar{\sigma}/\bar{\epsilon}$ determined. With D known, the theoretical strains can be calculated by equations (13) and (14) and the theoretical stress and strain components may then be plotted as shown in figure 7.

In order to show whether the ratios of the principal shear stresses to the principal shear strains are equal, as assumed by the deformation theory, values of the Lode variables μ and ν were computed (reference 5) and plotted as shown in figure 10. The theory requires that there be a straight-line relation between μ and ν but figure 10 shows that the test data depart appreciably from this straight-line relation. It should be noted that the values of μ and ν plotted in figure 10 are only approximate, since in the expressions used for these quantities it was assumed that the material was isotropic, the volume remained constant, and the plastic strains were relatively small.

VARIABLE-STRESS-RATIO TESTS WITHOUT UNLOADING

The foregoing constant-stress-ratio tests cannot determine whether the deformation or the flow theory agrees better with the test results, since for constant stress ratios the two theories coincide. For this reason, variable-stress-ratio tests were conducted by applying a stress in one direction followed by stressing in the other direction. Two sets of variable-stress-ratio tests were conducted: Set A, in which an axial tensile stress was applied followed by twisting moment, and set B, in which a twisting moment was applied followed by axial tension. In both series of tests, various initial amounts of straining in the plastic range were used. Nominal stress-strain diagrams for both the axial and torsional stresses are shown in figures 11 and 12. The manner of loading

and the amount of initial uniaxial stress and strain are also shown and the stage of loading is indicated by points labeled P_o, P_1, and P_2.

A comparison of the actual true plastic stress-strain relations with the theoretical relations as given by the deformation and flow theories for tests of both set A and set B is shown in figures 13 and 14. The determination of the theoretical values for the deformation based on the uniaxial tension test results is described above. The theoretical values based on the flow theory were computed in a manner similar to that described by Shepherd (reference 6). From figures 13 and 14, no definite conclusion can be made as to which theory agrees better with the actual test results. Figures 13 and 14, however, do show that there is better agreement between either theory and the test results for the range of small strains than for large strains.

The foregoing variable-stress-ratio tests can also be used to distinguish between the deformation and the flow-type theory. In order to make the foregoing distinctions, the loading paths used in the tests will first be summarized as indicated in figure 15. In figure 15 one set of tests, designated as set A, corresponds to loading in the axial direction to a stress σ_x corresponding to specified offset strain values (for example, as represented by point B) and then loading to points 1, 6, 11, 16, and 21 in torsion. Another set of tests, designated as set B, corresponds to loading, for example, in torsion to a stress $\tau_{xy} = \sigma_x/2$ as represented by point A and then loading to points 1, 2, 3, 4, and 5 in axial tension. The values used were equal to those used for set A. According to the deformation-type theory, the axial and transverse strains corresponding to point 1 are the same, regardless of whether the loading path was OA1 or OB1. The first line in table 2 shows the strains in the axial and transverse directions for each path of loading and the percentage difference in these strains. Table 2 also shows the percentage difference for points 1 to 25. The percentage difference in strains for the two different paths of loading lends support to the flow-type theory rather than the deformation-type theory. This appears to be the correct conclusion since the large percentage differences in strain given in table 2 cannot be explained by the anisotropy of the material.

SPECIAL UNLOADING TESTS TO CHECK ASSUMPTION OF ISOTROPIC STRAIN-HARDENING

It is assumed in the isotropic linear flow theories that initial prestraining will not produce anisotropy. In other words, it is assumed

that isotropic strain-hardening occurs. To determine the accuracy of this assumption a test was made in which a specimen was stressed first in the axial direction to a specified strain value. This axial stress was then removed and the specimen was then stressed in torsion until failure occurred. Another specimen was initially stressed in torsion to an equivalent initial strain value as used in the first specimen. The torsional stress was then removed and axial tension stress was applied to failure. For the assumption of isotropic strain-hardening to be valid, the significant stress-strain curves for each of the foregoing tests should coincide.

Tests were made as described in the foregoing discussion for four initial significant strains of values $\bar{\epsilon} = 0.005$, 0.01, 0.02, and 0.04 inch per inch. The nominal stress-strain relations for these tests are shown in figure 16. For the test results with the initial stress in torsion, nominal stress-strain relations as given in figure 17 were obtained.

True stress-strain relations corresponding to the nominal stress-strain relations in figures 16 and 17 are shown in figure 18. Based on the true stress-strain relations in figure 18 and using the equations for the significant stress and strain, the significant stress-strain relations plotted in figure 19 were prepared. Comparisons can be made in figure 19 between tests with the same amount of initial prestraining where the prestraining was in different directions. A comparison of the graphs in figure 19 shows that the assumption of isotropic strain-hardening does not appear to be valid. The conclusion based on figure 19, however, may not be conclusive since the initial anisotropy of the material is not considered in these graphs. To eliminate the influence of the initial anisotropy, figures 20(a) and 20(b) were prepared showing the significant stress-strain relations for axial tension and circumferential tension. Since the significant stress-strain data for the special tests do not fall between the simple-tension stress-strain curves in figure 20, it appears that the assumption of isotropic strain-hardening does not apply.

SPECIAL TESTS TO CHECK ASSUMPTION THAT DIRECTIONS OF PRINCIPAL STRESSES AND STRAINS COINCIDE

Tests were conducted to determine whether the directions of the principal stresses and strains coincide during plastic flow under conditions where the principal stress ratio varies. For this purpose two tests were conducted, one in which axial tension was applied to a specified amount followed by torsion and the other where torsion was applied followed by axial tension. In both tests, an SR-4 strain

rosette was used to measure the magnitudes and directions of the principal strains. For each load increment the directions of the principal stresses could also be calculated. The angles shown in figure 21 define the directions of principal stress and principal strain for each test and for various points during loading. The difference in the angles shown in figure 21 indicates that the directions of the principal stress and strain cannot be assumed to coincide. However, the resulting error in making this assumption may not be important as shown in figure 22. Figure 22 shows the error in principal strain values assuming principal strains to be in the direction of the principal stresses. The percentage difference between the strain values is small and amounts to a maximum of 2.5 percent.

CONCLUSIONS

For the 14S-T4 aluminum alloy tested under combined tension and torsion the following conclusions can be made:

1. Constant-stress-ratio tests show approximate agreement between actual plastic stress-strain relations and those predicted by the flow and deformation theories.

2. Variable-stress-ratio test results do not agree with either the flow or the deformation theory.

3. Variable-stress-ratio tests using different paths of loading but resulting in the same final loading condition show different final strains and hence these tests support the flow theory rather than the deformation theory.

4. Special unloading tests indicate that the assumption of isotropic strain-hardening is not valid.

5. Variable-stress-ratio tests were made that showed an appreciable difference between the directions of the principal stresses and strains. However, the strains in the directions of the principal stresses agree well with the principal strain values.

The Pennsylvania State College
State College, Pa., September 1, 1951

REFERENCES

1. Marin, Joseph, Faupel, J. H., Dutton, V. L., and Brossman, M. W.: Biaxial Plastic Stress-Strain Relations for 24S-T Aluminum Alloy. NACA TN 1536, 1948.

2. Marin, Joseph, Ulrich, B. H., and Hughes, W. P.: Plastic Stress-Strain Relations for 75S-T6 Aluminum Alloy Subjected to Biaxial Tensile Stresses. NACA TN 2425, 1951.

3. Marin, Joseph: Stress-Strain Relations in the Plastic Range for Biaxial Stresses. Jour. Franklin Inst., vol. 248, no. 3, Sept. 1949, pp. 231-249.

4. Prager, W.: Strain Hardening under Combined Stresses. Jour. Appl. Phys., vol. 16, no. 12, Dec. 1945, pp. 837-840.

5. Nádai, Arpád: Theory of Flow and Fracture of Solids. Vol. I. Second ed., McGraw-Hill Book Co., Inc., 1950.

6. Shepherd, W. M.: Plastic Stress-Strain Relations. Proc. Institution Mech. Eng., vol. 159, 1948, pp. 95-99; discussion, pp. 99-114. (Formerly War Emergency Issue No. 39.)

TABLE 1

YIELD STRESSES FOR VARIOUS RATIOS OF BIAXIAL STRESSES

Stress ratio, $R = \frac{\sigma_2}{\sigma_1}$	Maximum principal yield stress, σ_{1y}	Minimum principal yield stress, σ_{2y}	Stress ratios	
			$x = \frac{\sigma_{1y}}{\sigma_y}$	$y = \frac{\sigma_{2y}}{\sigma_y}$
0	35,600	-------	1.00	0
-.20	32,400	-6,600	.91	-.19
-.46	25,300	-11,600	.71	-.33
-.73	22,700	-16,500	.64	-.46
-1.0	21,200	-21,200	.60	-.60

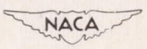

TABLE 2

COMPARISON OF TRUE STRAINS USING DIFFERENT LOADING PATHS

Point	True axial strain (in./in.)				True shear strain (in./in.)			
	Set A (1)	Set B (2)	Difference In./in.	Difference Percent (3)	Set A (1)	Set B (2)	Difference In./in.	Difference Percent (3)
1	0.0040	0.0052	0.0012	23	0.0049	0.0083	0.0034	41
2	.0052	.0067	.0015	22	.0056	.0097	.0041	42
3	.0082	.0116	.0034	29	.0078	.0133	.0055	41
4	.0262	.0370	.0108	29	.0260	.0209	-.0051	-24
5	.0319	.0424	.0105	25	.0309	.0350	.0049	14
6	.0041	.0056	.0015	28	.0063	.0092	.0029	32
7	.0052	.0081	.0029	36	.0079	.0107	.0028	26
8	.0085	.0122	.0037	30	.0120	.0146	.0026	18
9	.0290	.0389	.0099	25	.0353	.0233	-.0120	-52
10	.0352	.0441	.0089	20	.0419	.0211	-.0208	-99
11	.0050	.0077	.0027	35	.0088	.0149	.0061	41
12	.0069	.0115	.0046	40	.0111	.0180	.0069	38
13	.0108	.0159	.0051	32	.0261	.0221	-.0040	-18
14	.0361	.0461	.0100	22	.0441	.0325	-.0116	-36
15	.0435	.0501	.0066	13	.0519	.0296	-.0223	-75
16	.0072	.0138	.0066	48	.0165	.0310	.0145	47
17	.0101	.0200	.0099	50	.0204	.0377	.0163	43
18	.0163	.0253	.0090	36	.0295	.0419	.0124	30
19	.0323	.0634	.0311	49	.0723	.0568	-.0155	-27
20	.0381	.0637	.0256	40	.0830	.0562	-.0268	-48
21	.0103	.0154	.0051	33	.0252	.0359	.0107	30
22	.0139	.0226	.0087	38	.0307	.0440	.0133	30
23	.0205	.0280	.0075	27	.0415	.0480	.0065	14
24	.0499	.0784	.0285	36	.0875	.0638	-.0237	-37
25	.0588	.0675	.0087	13	.0978	.0652	-.0326	-50

[1]Initially stressed in σ_x direction.

[2]Initially stressed in τ_{xy} direction.

[3]Percentage differences shown are based on set B strain values.

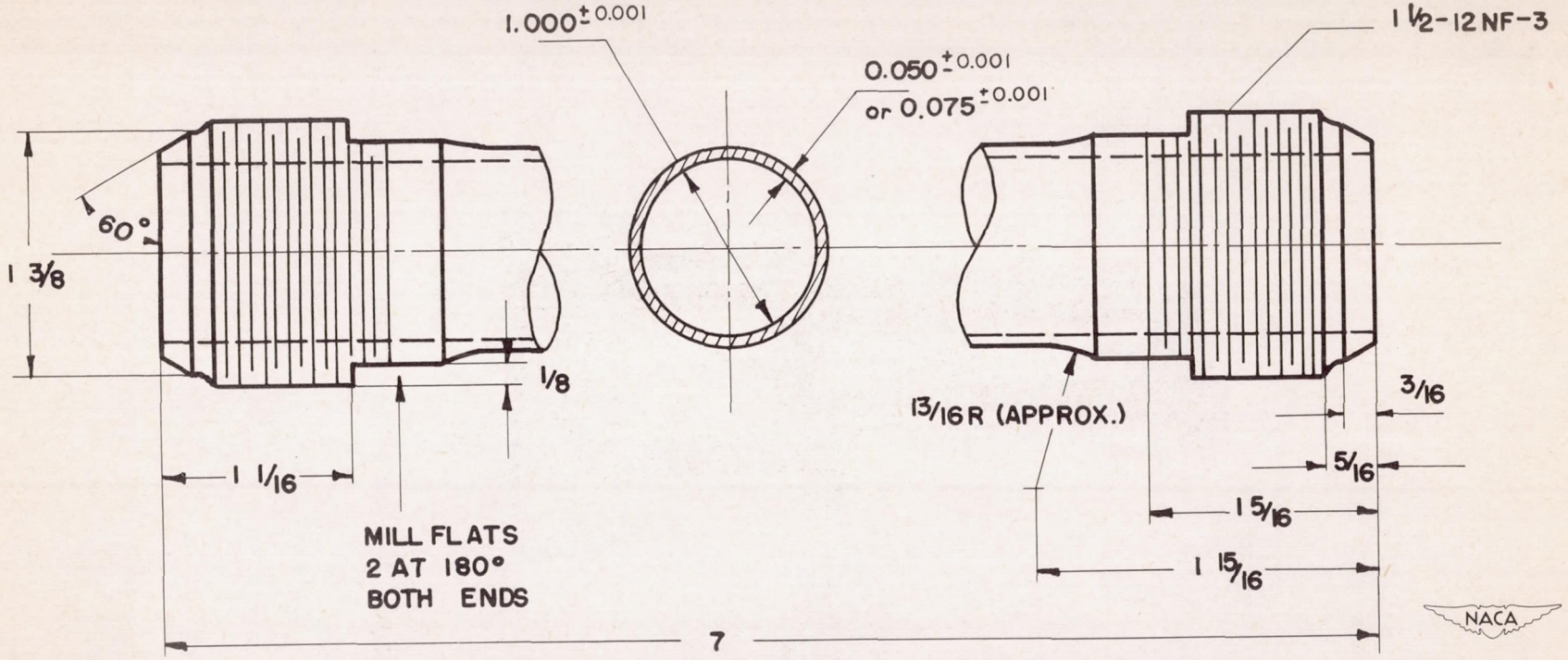

Figure 1.- Biaxial stress specimen. All dimensions are in inches. Inner and outer surfaces of tube must be polished smooth with 9/0 Metalite cloth.

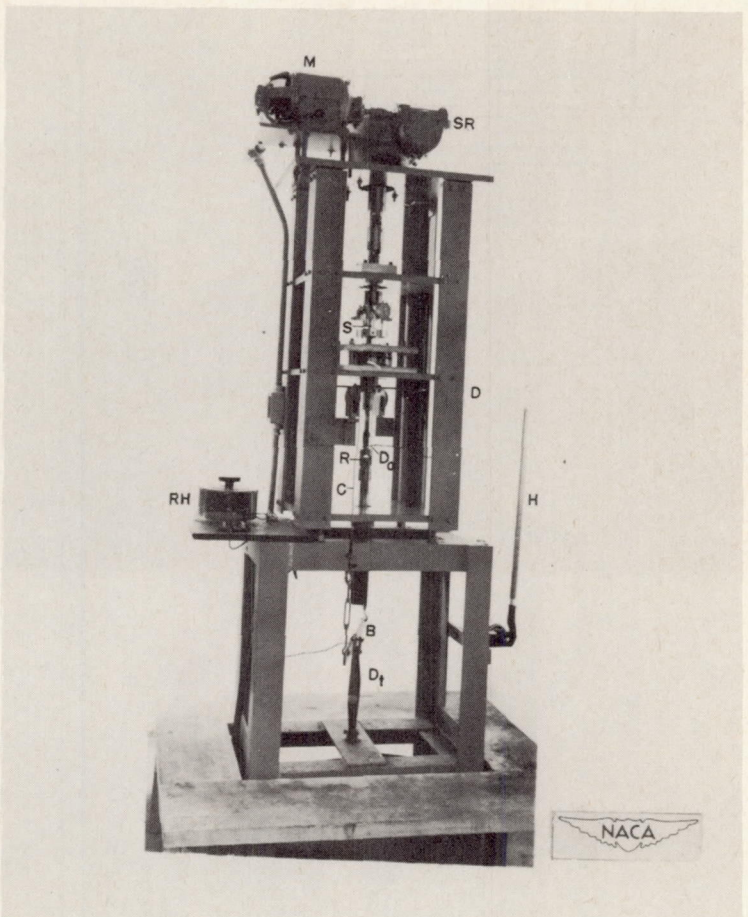

Figure 2.- Tension-torsion testing machine.

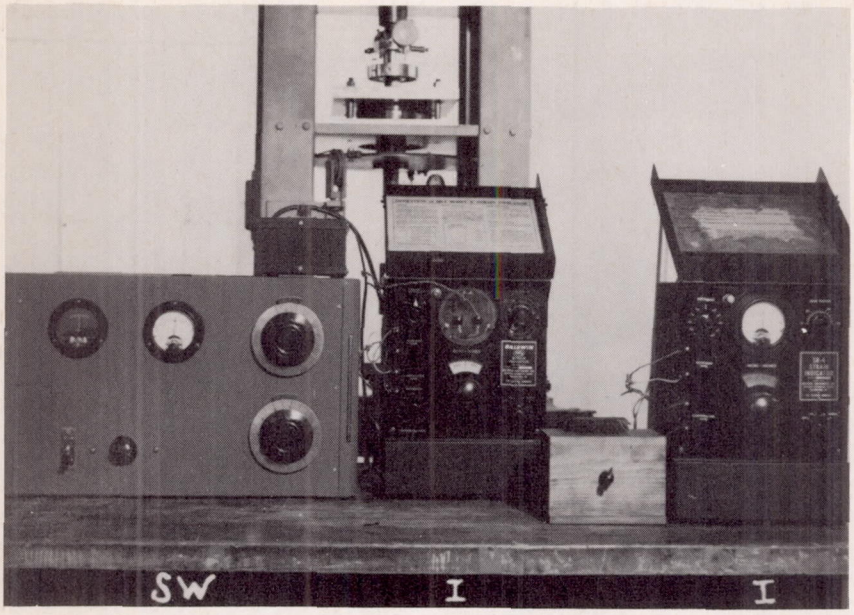

Figure 3.- Strain-indicating and switching unit.

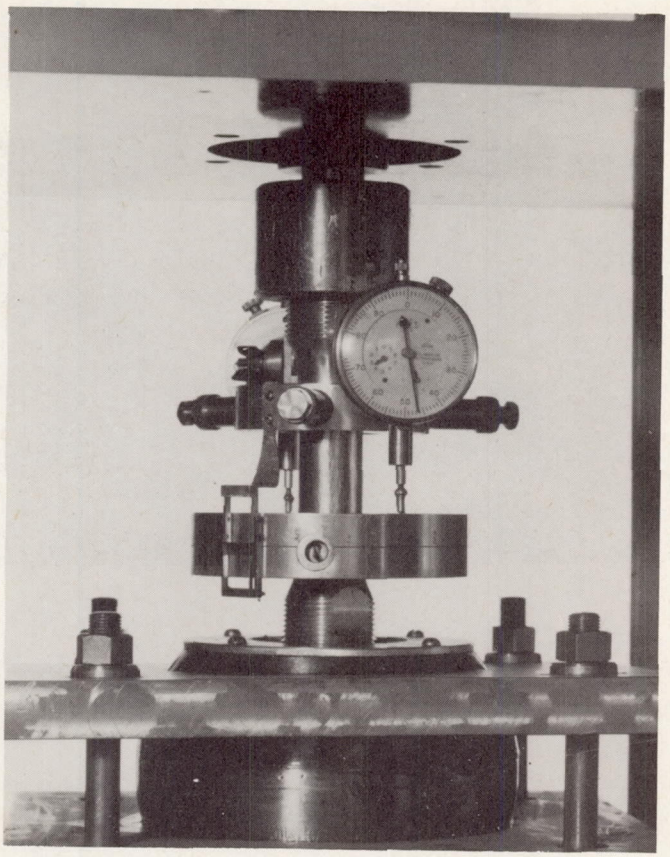

Figure 4.- Tension-torsion strain gage.

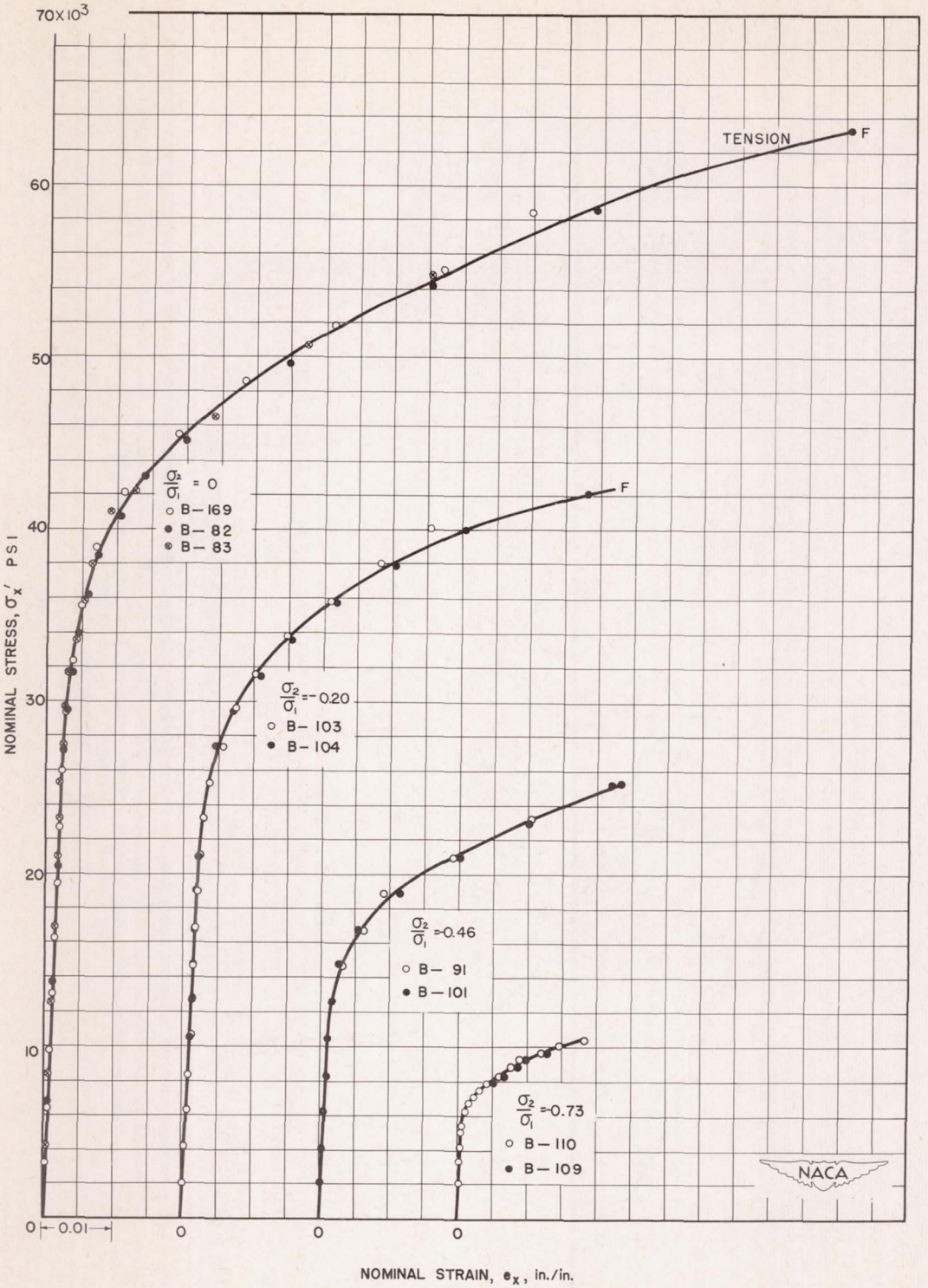

(a) Nominal axial stress and strain.

Figure 5.- Stress-strain relations for constant-stress-ratio tests. F denotes fracture.

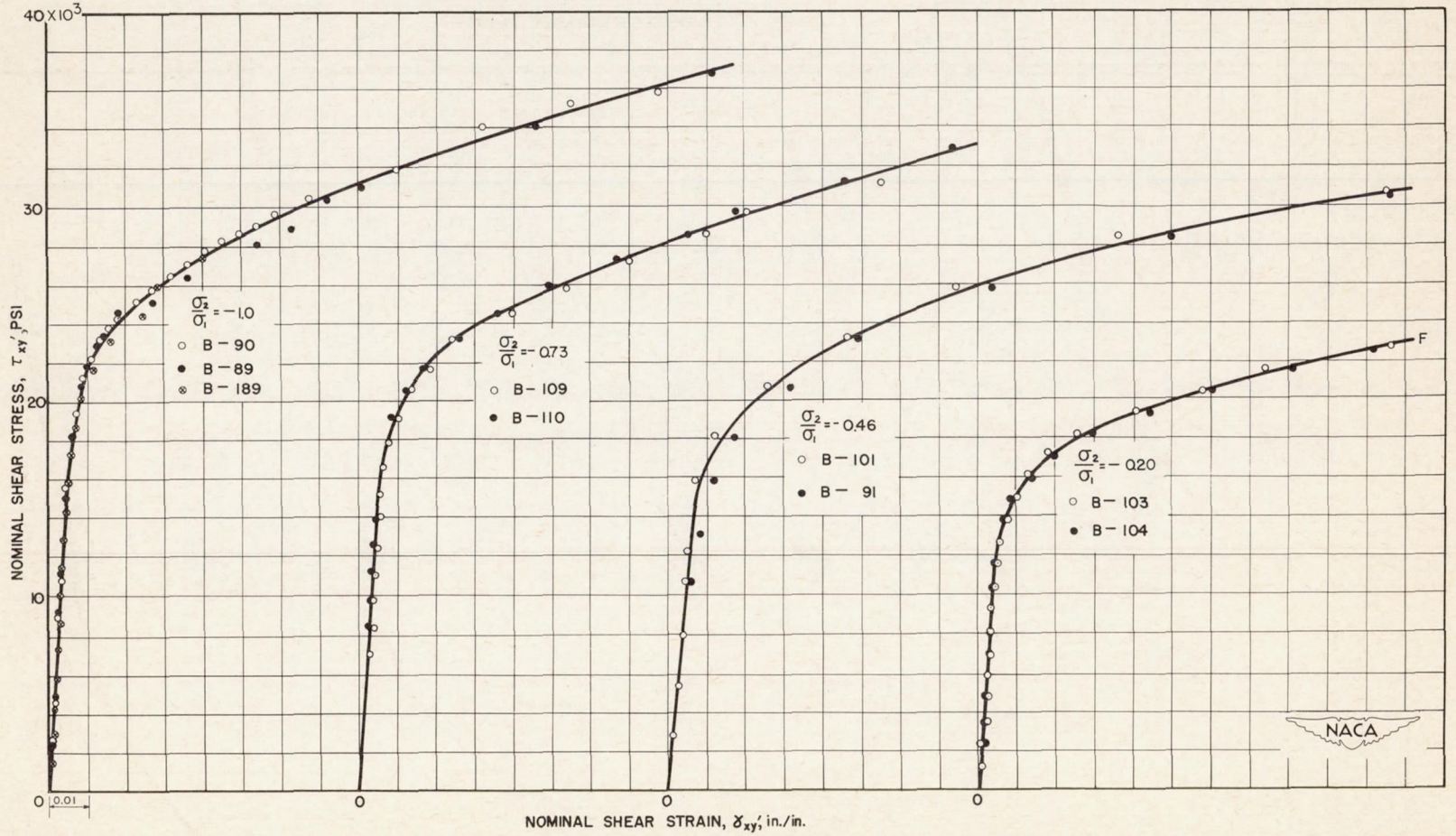

(b) Nominal shear stress and strain.

Figure 5.- Concluded.

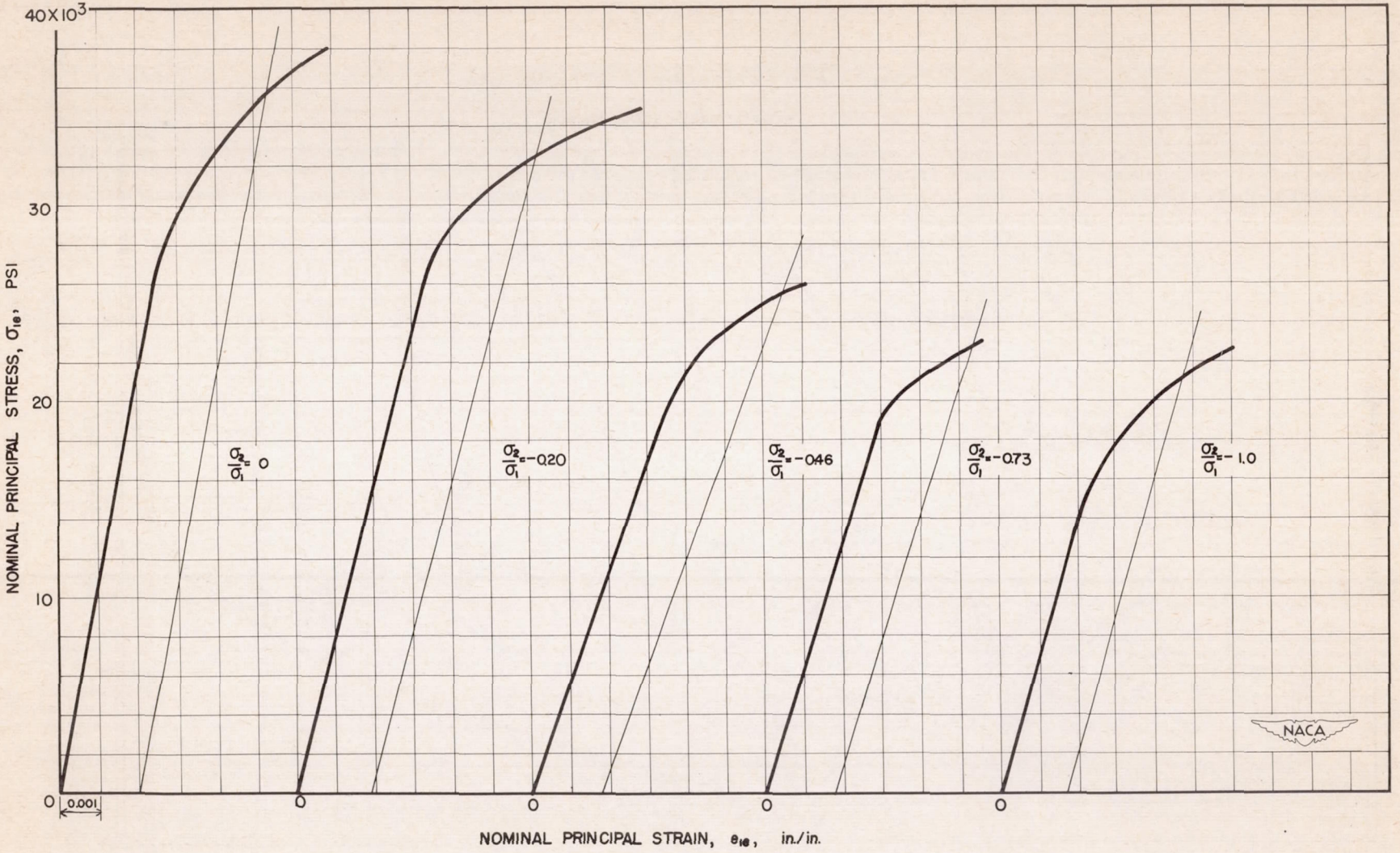

(a) For maximum principal stress.

Figure 6.- Elastic stress-strain relations for constant-stress-ratio tests.

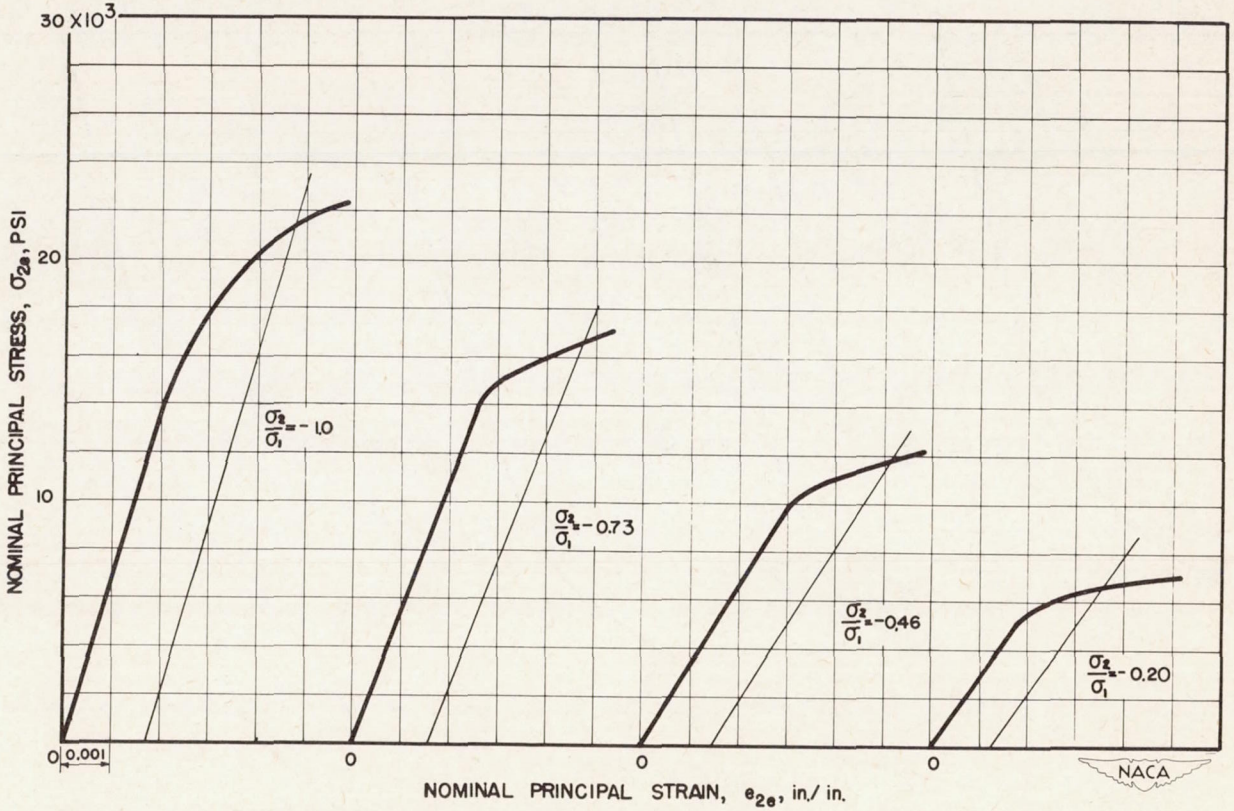

(b) For minimum principal stress.

Figure 6.- Concluded.

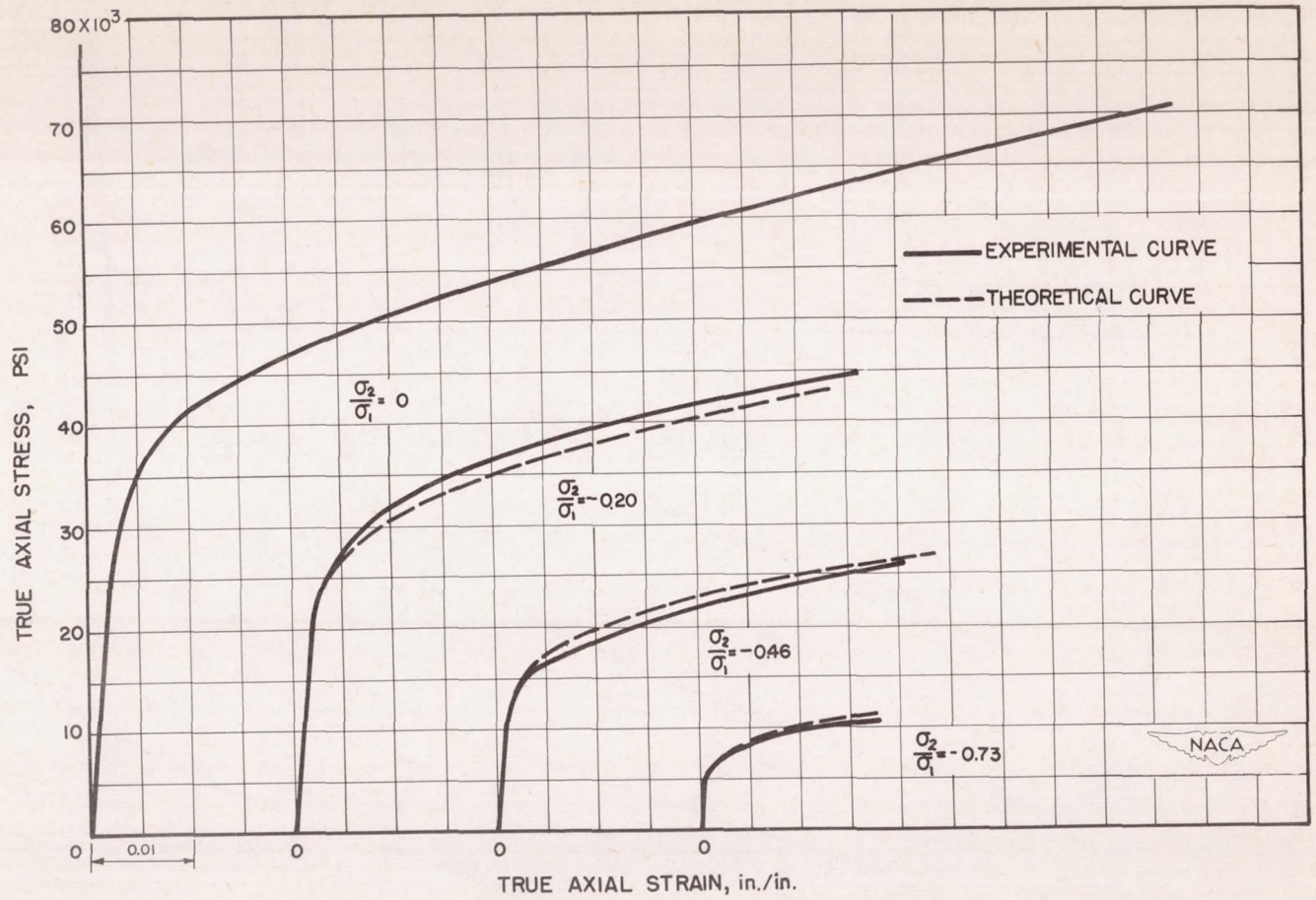

(a) True axial stress and strain.

Figure 7.- Comparison of true plastic stress-strain relations with deformation theory for constant stress ratios.

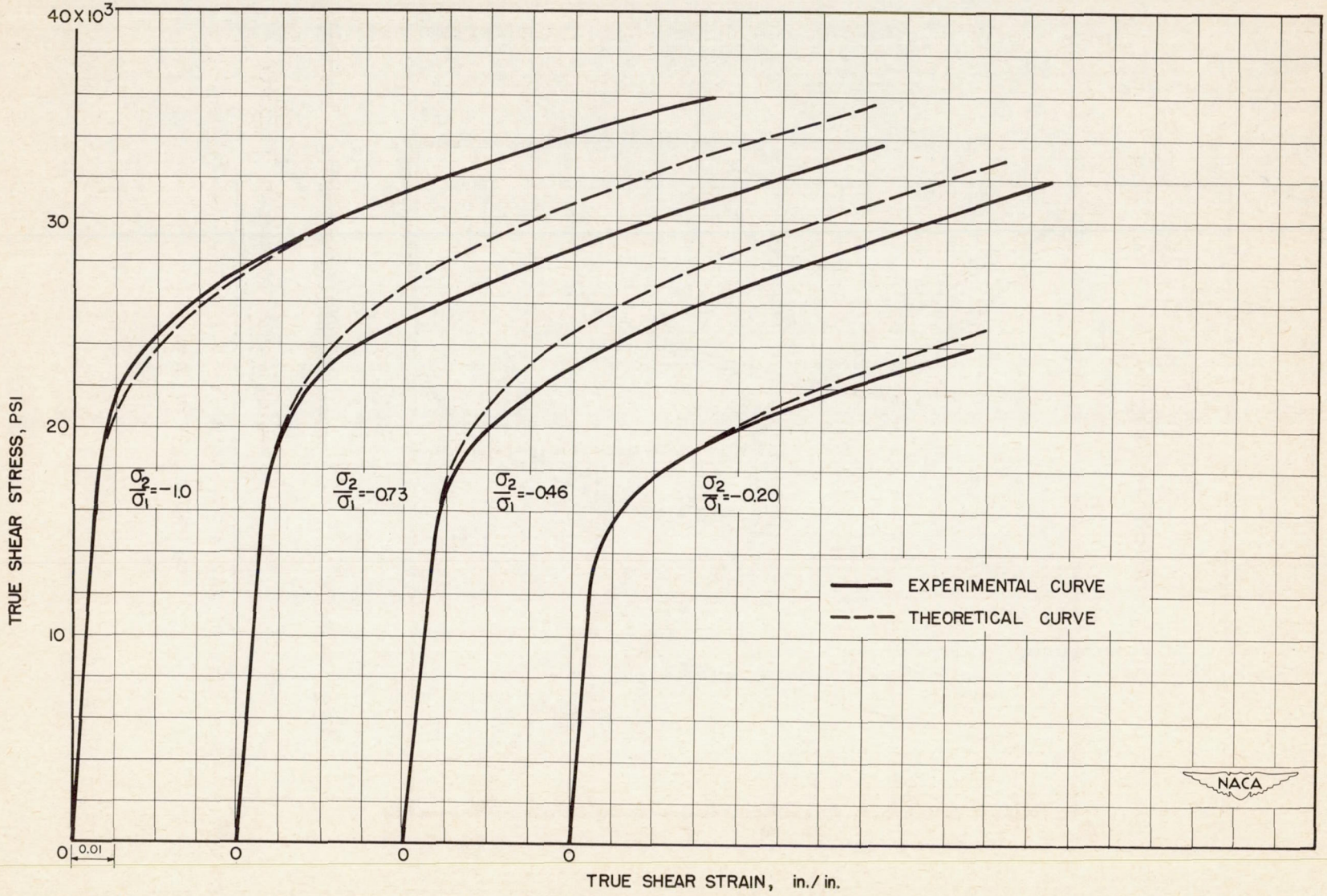

(b) True shear stress and strain.

Figure 7.- Concluded.

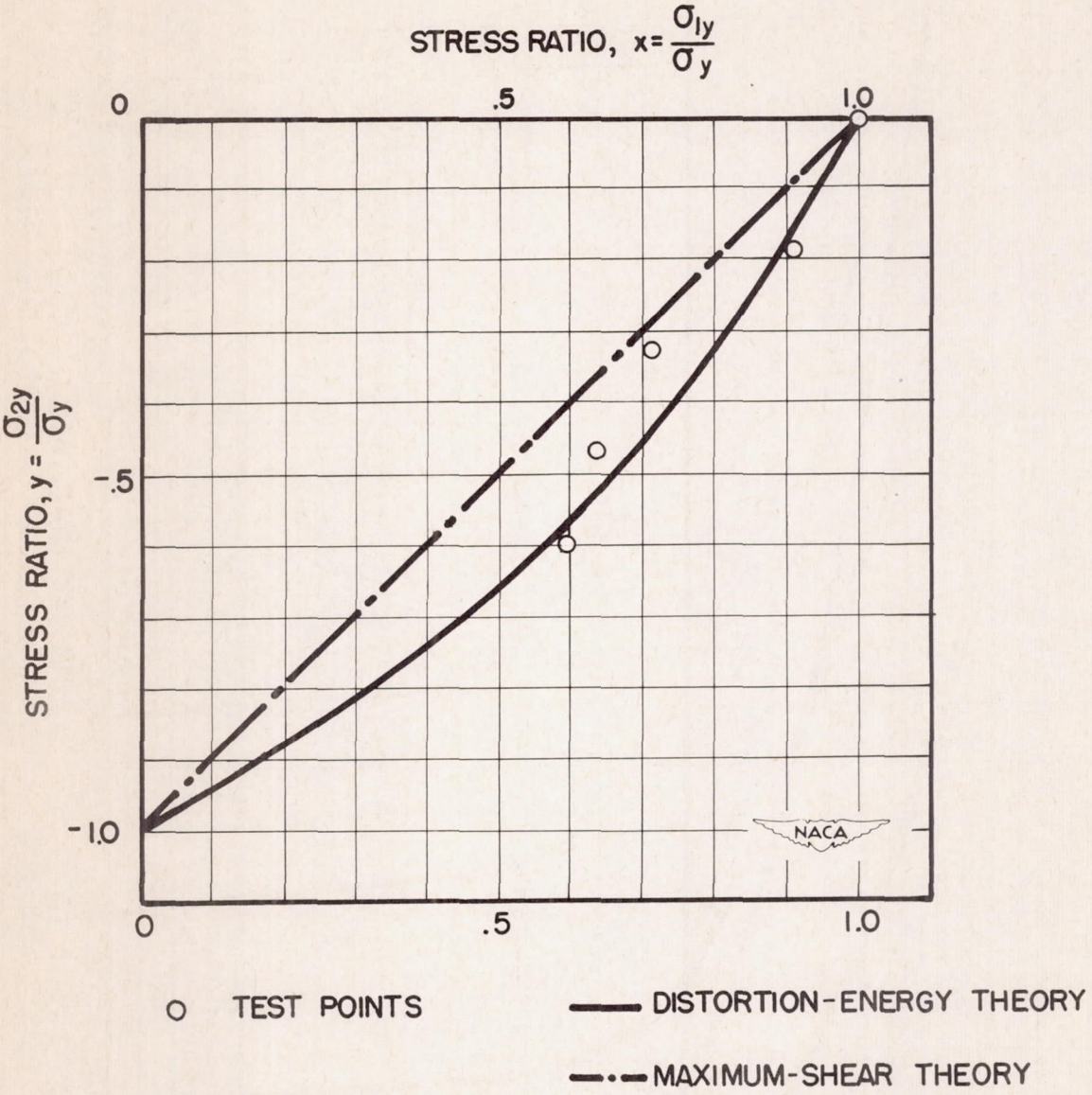

Figure 8.- Comparison of yield strengths with theories of failure.

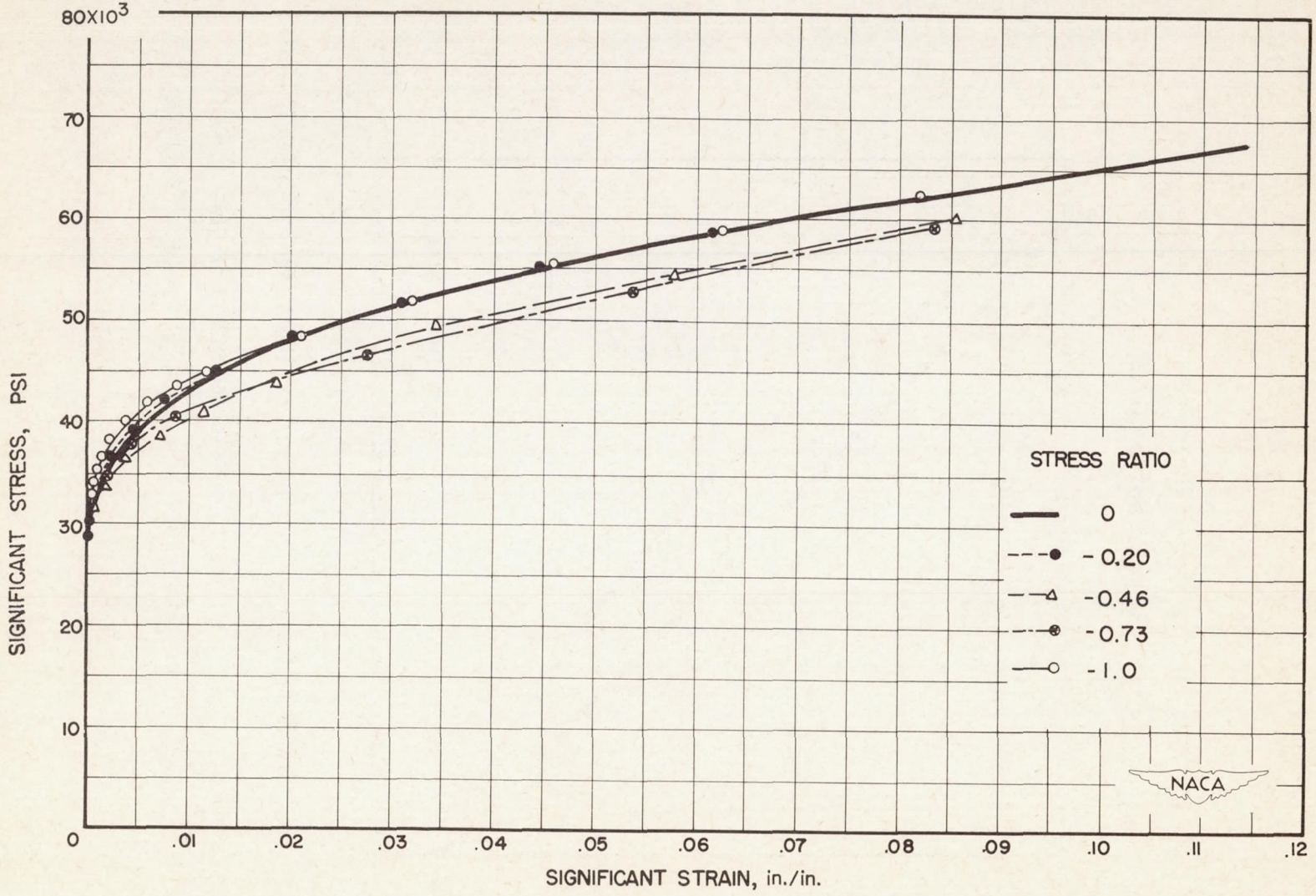

Figure 9.- Comparison of significant stress-strain relations with uniaxial stress-strain values for constant-stress-ratio tests.

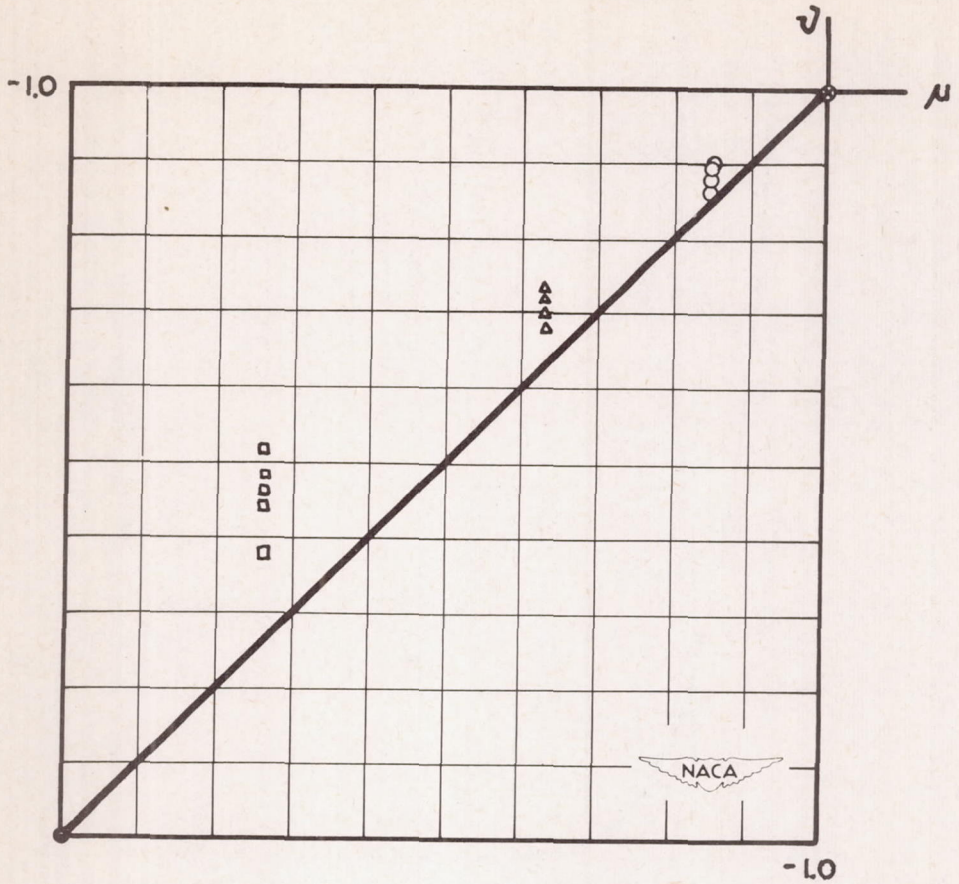

Figure 10.- Plot of μ against ν for constant-stress-ratio tests.

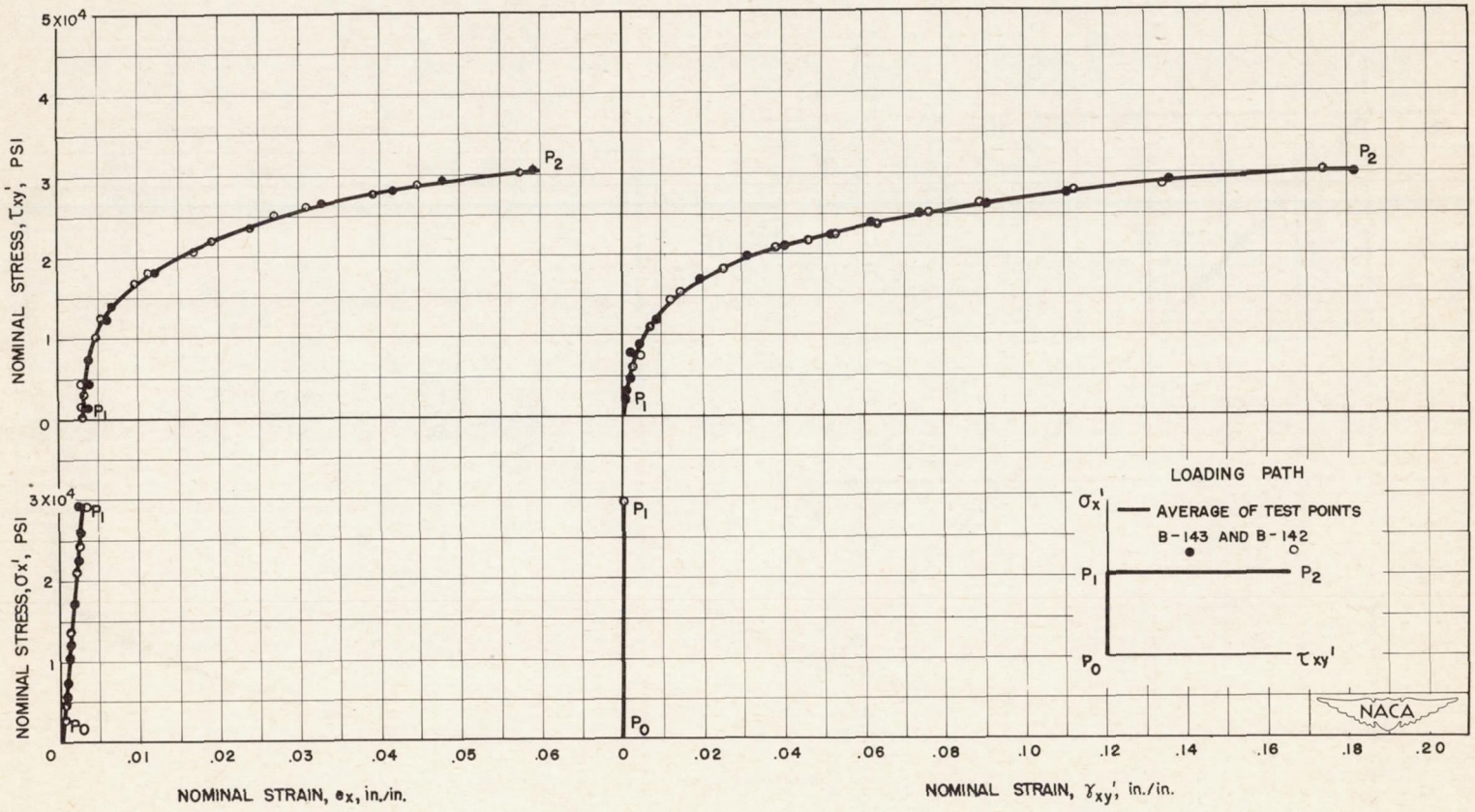

(a) Set A, test 1.

Figure 11.- Nominal stress-strain relations for variable-stress-ratio tests.
F denotes fracture.

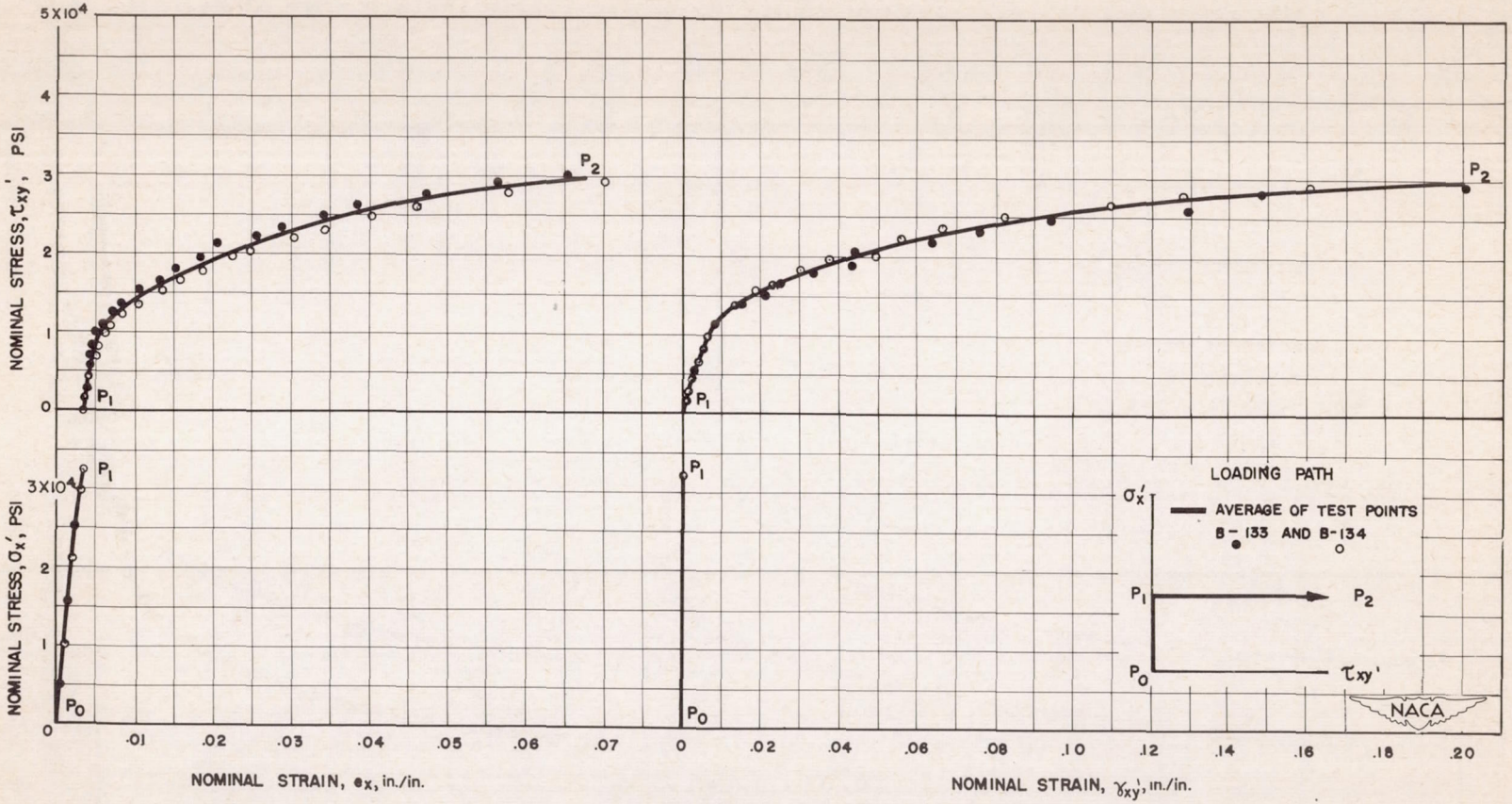

(b) Set A, test 2.

Figure 11.- Continued.

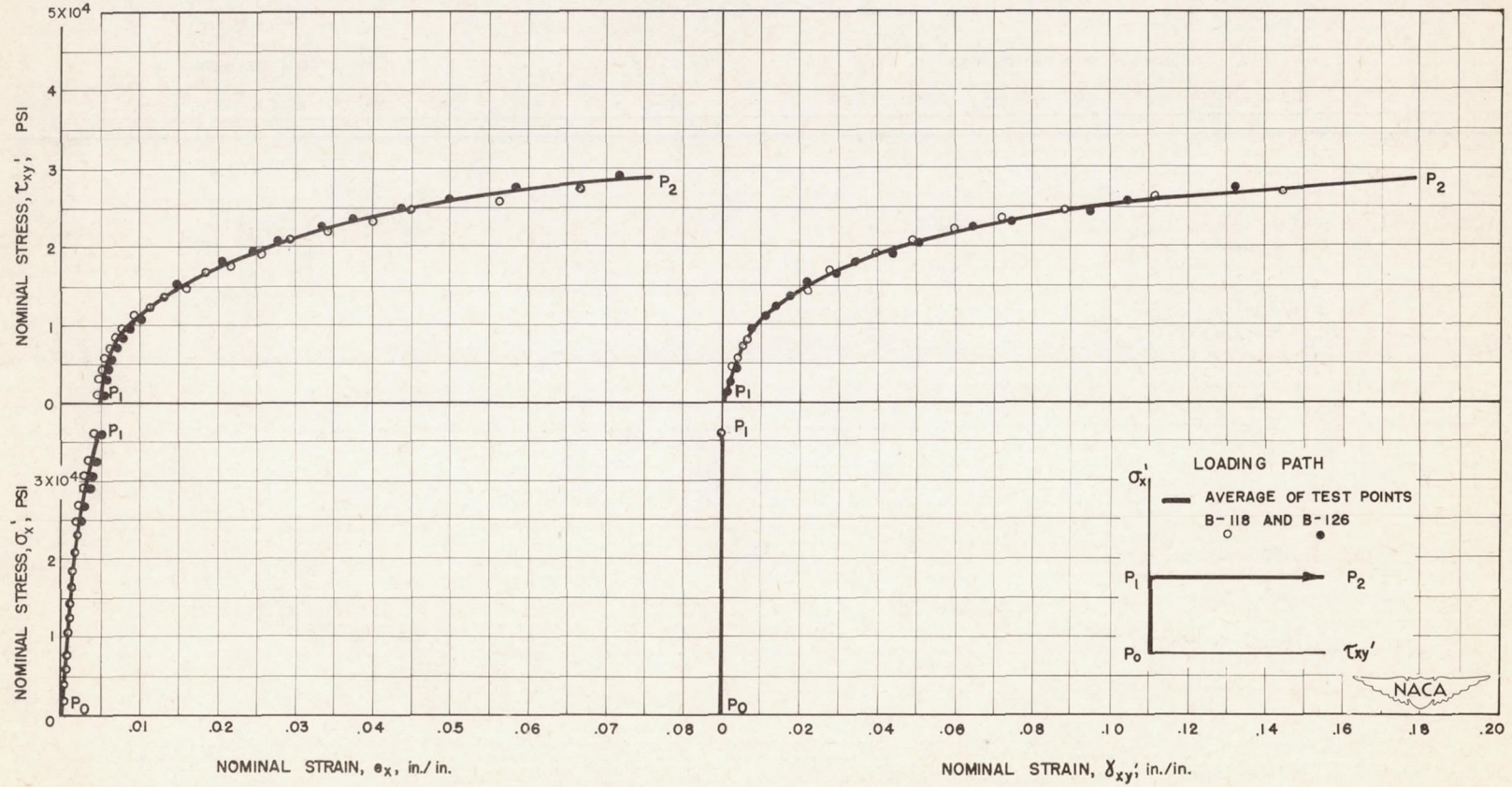

(c) Set A, test 3.

Figure 11.- Continued.

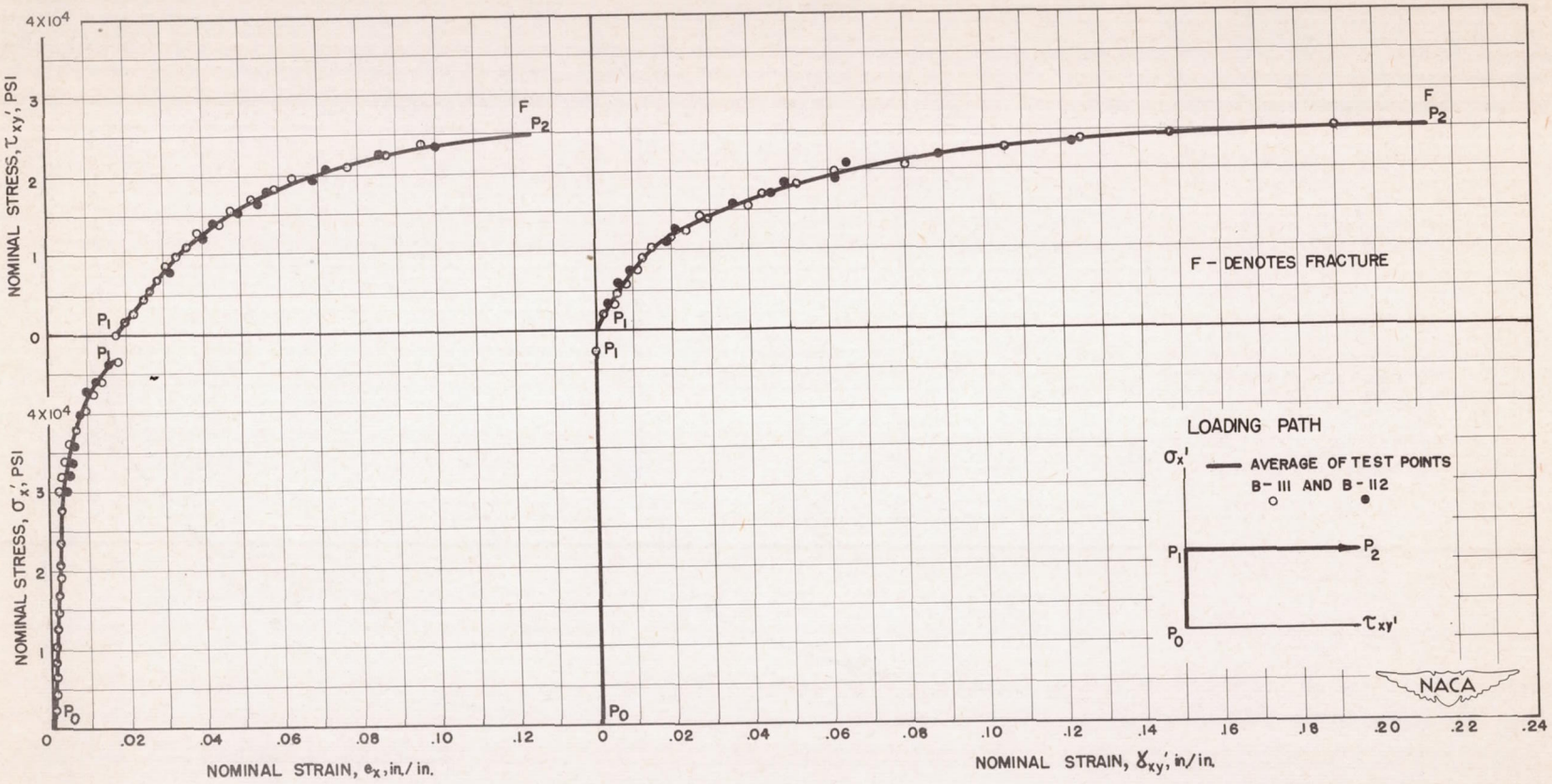

(d) Set A, test 4.

Figure 11.- Continued.

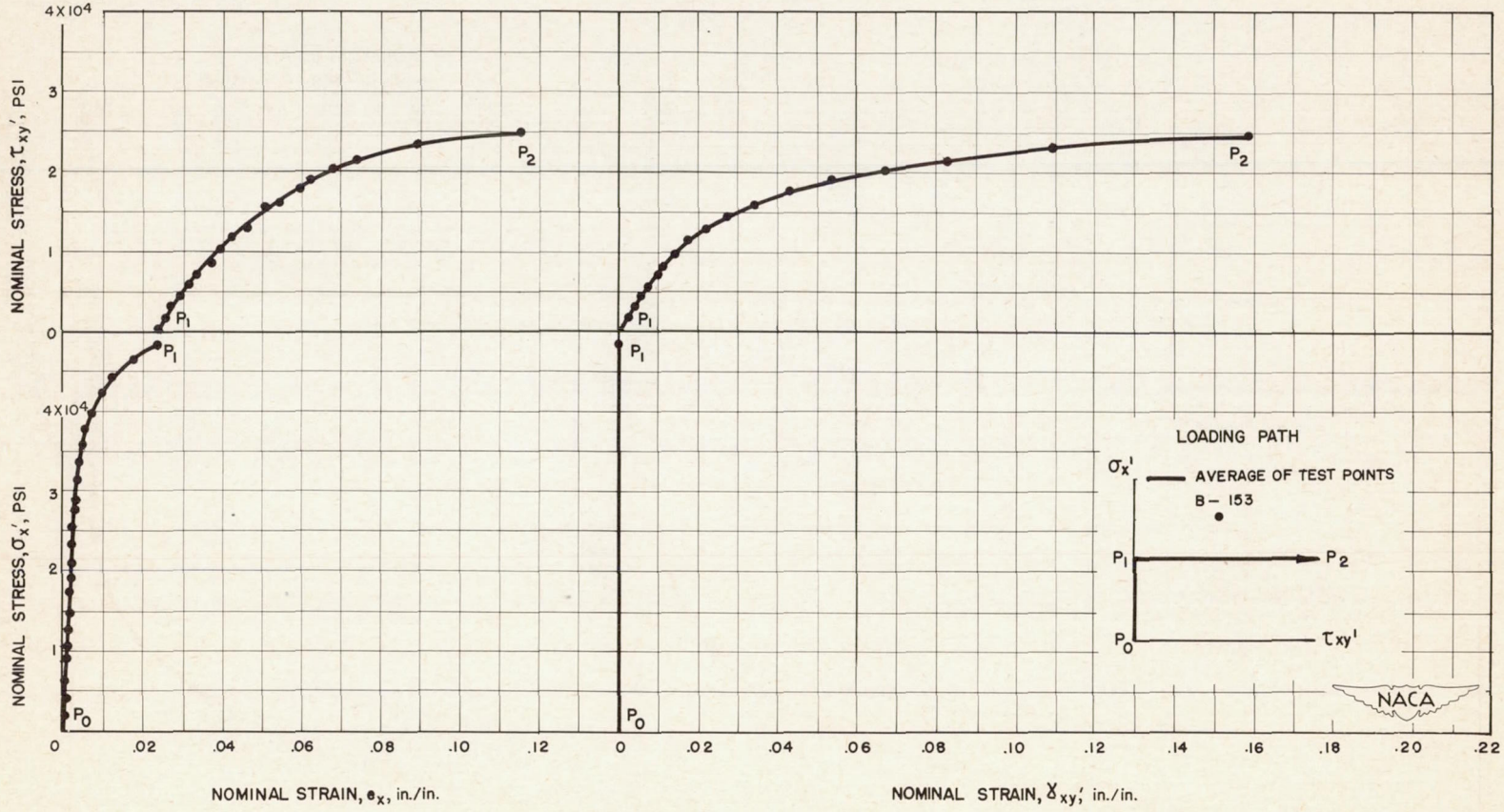

(e) Set A, test 5.

Figure 11.- Concluded.

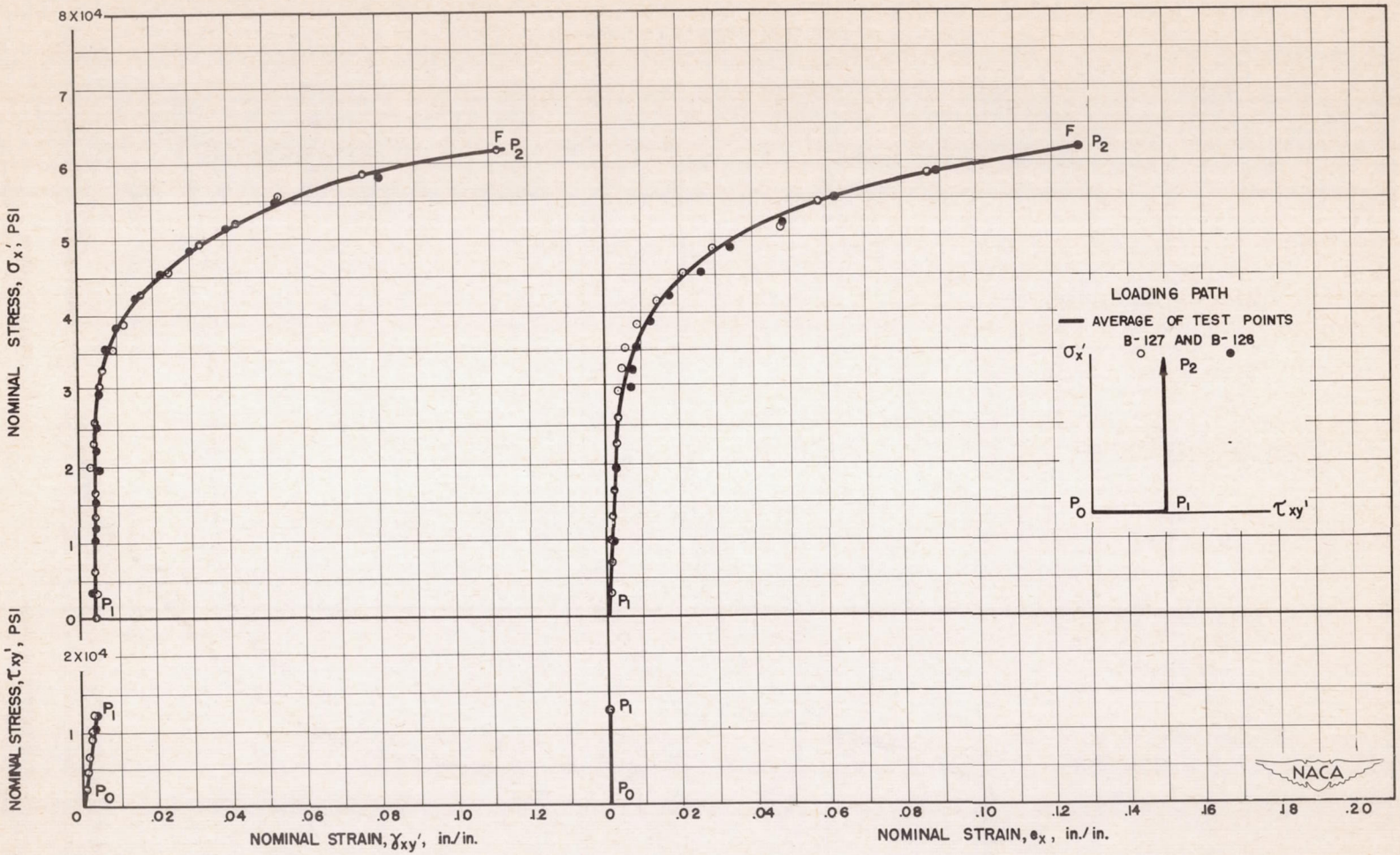

(a) Set B, test 1.

Figure 12.- Nominal stress-strain relations for variable-stress-ratio tests.
F denotes fracture.

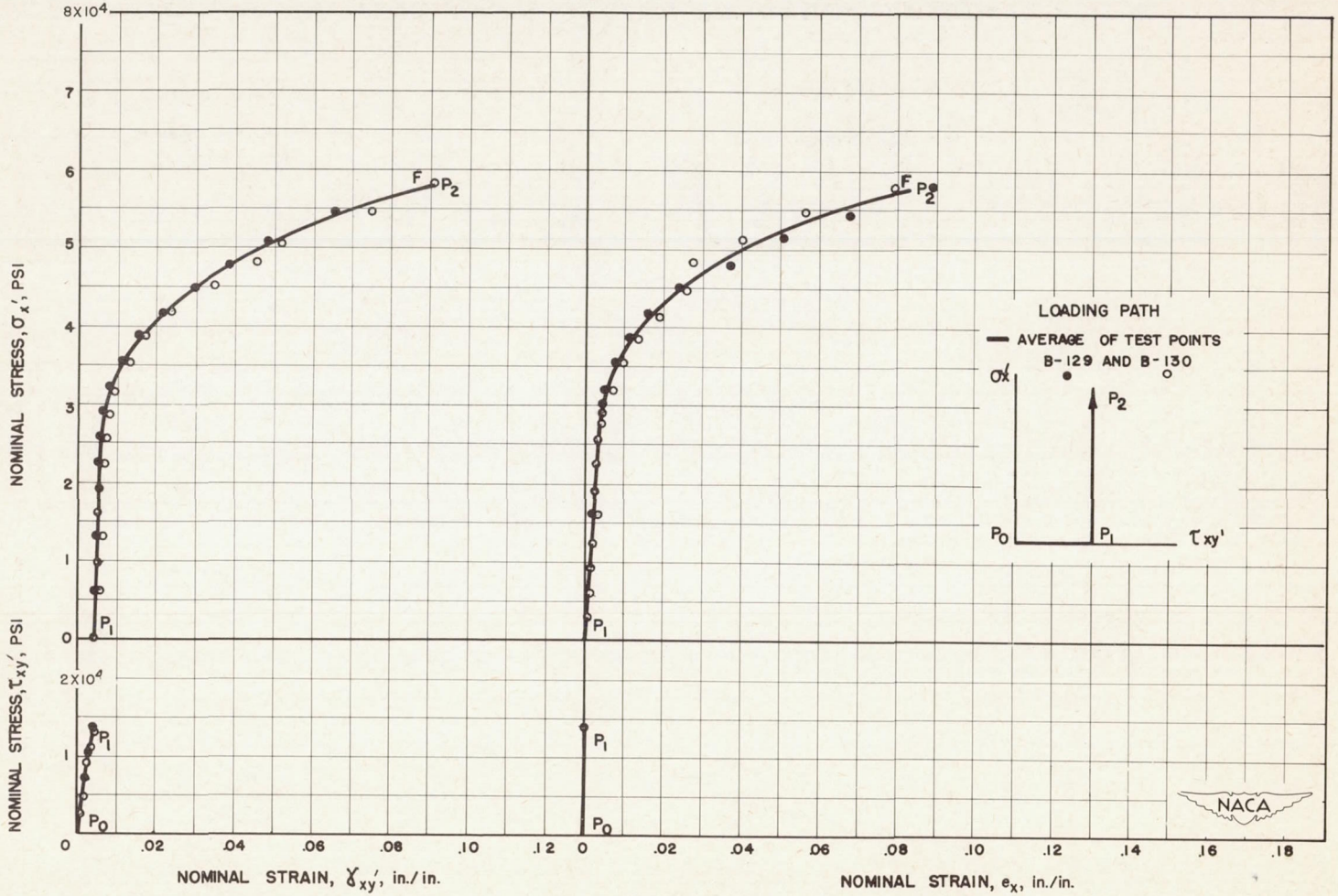

(b) Set B, test 2.

Figure 12.- Continued.

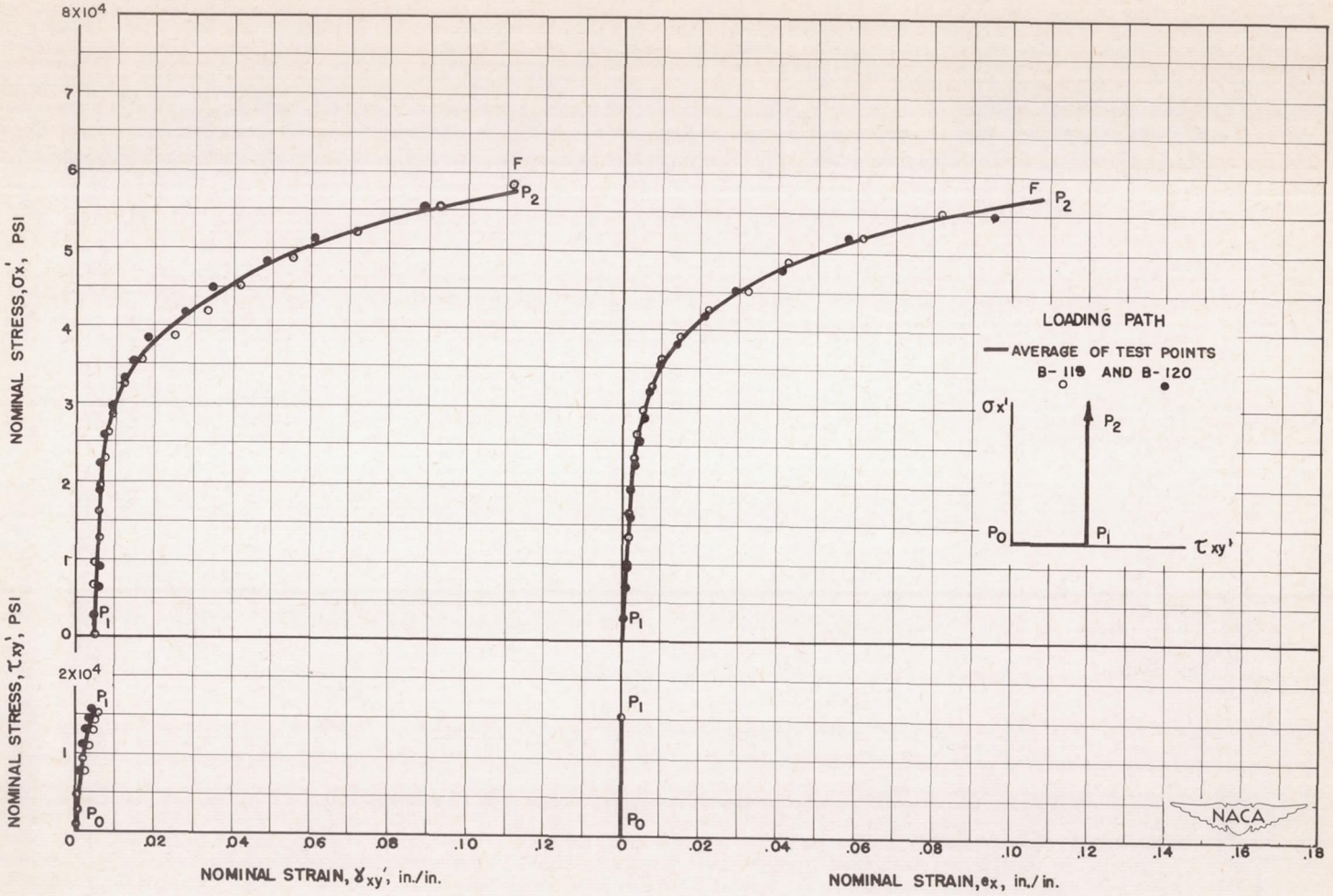

(c) Set B, test 3.

Figure 12.- Continued.

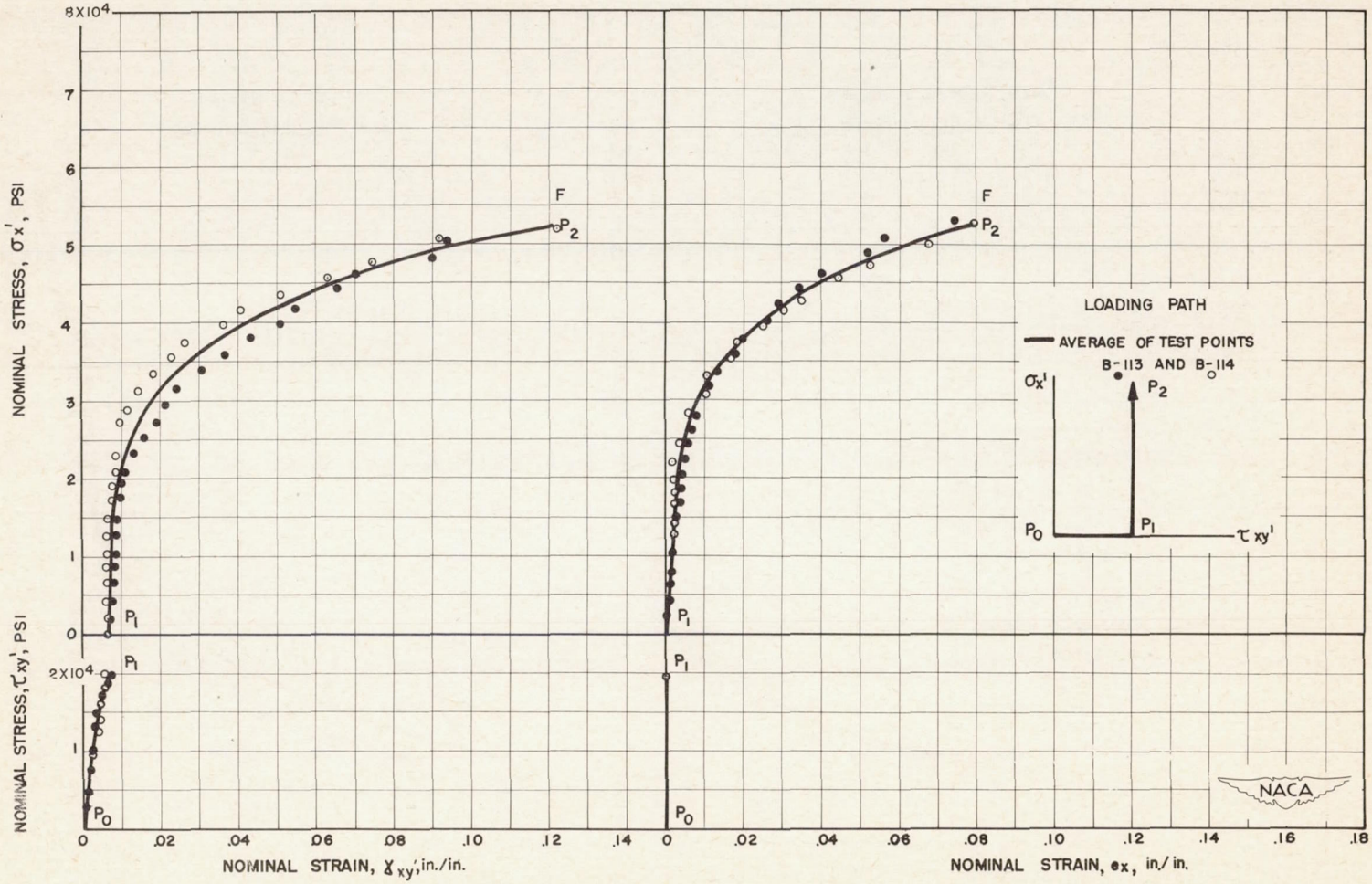

(d) Set B, test 4.

Figure 12.- Continued.

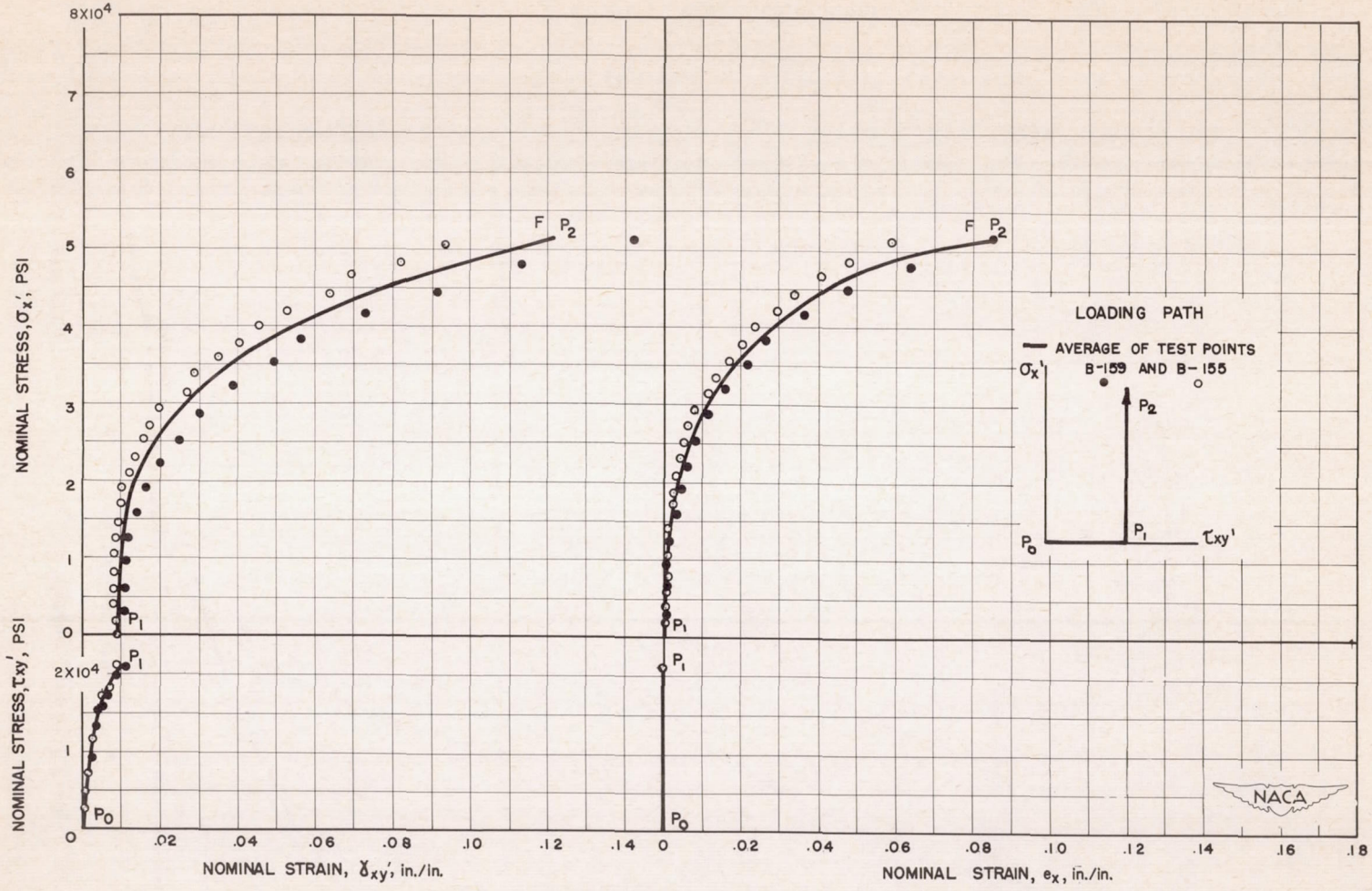

(e) Set B, test 5.

Figure 12.- Concluded.

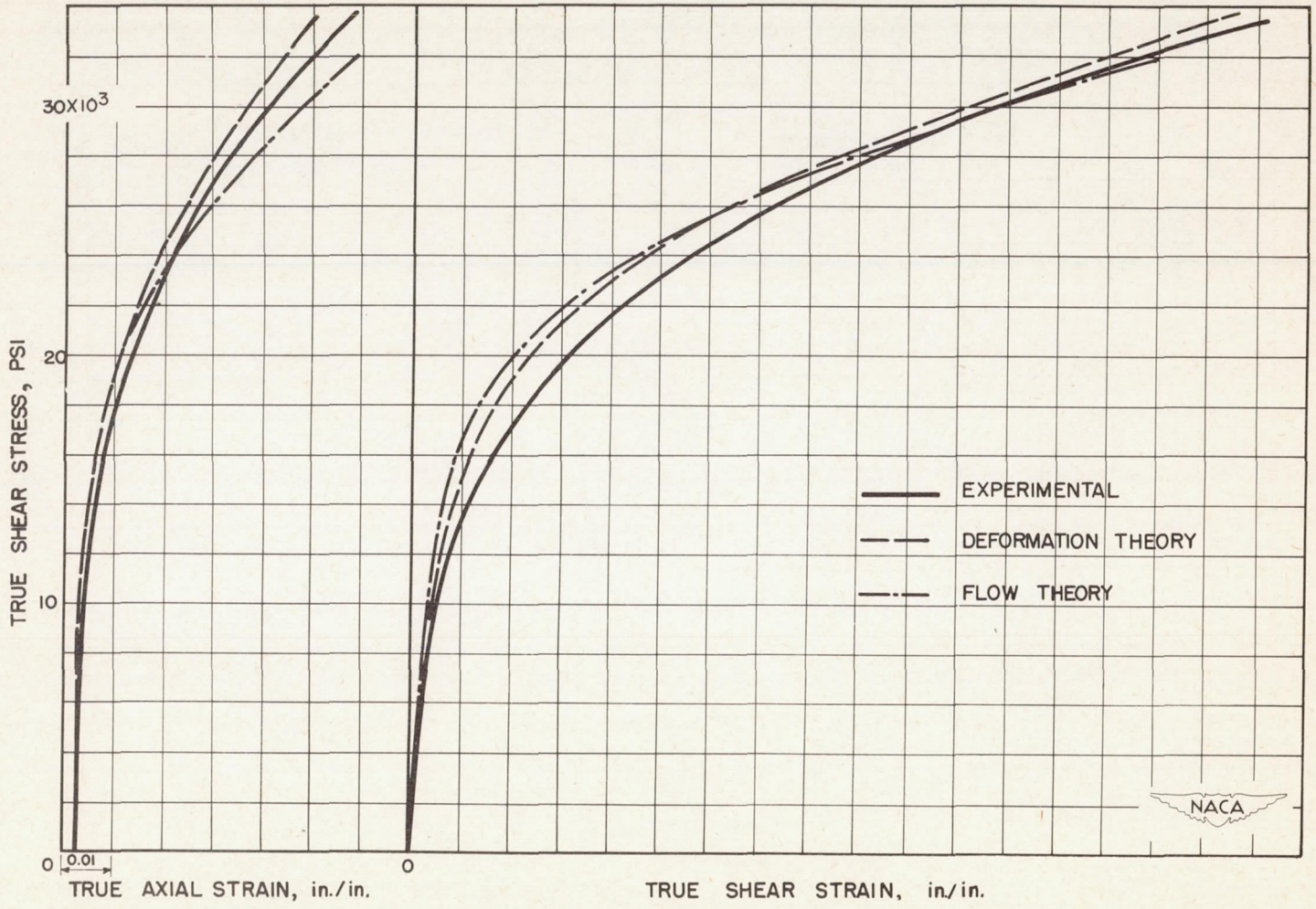

(a) Set A, test 1.

Figure 13.- Comparison of true stress-strain diagrams with plasticity theories for variable-stress-ratio tests.

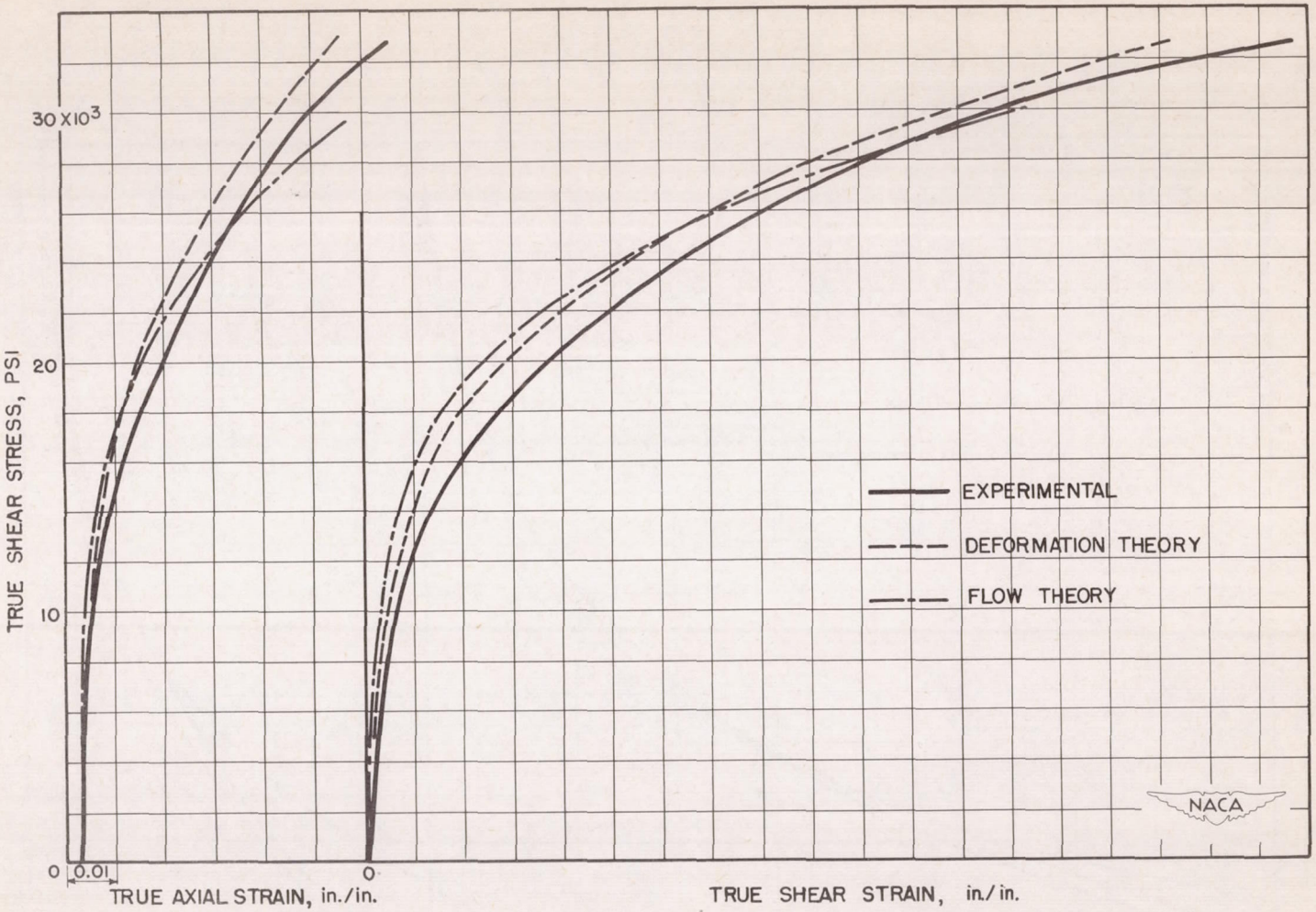

(b) Set A, test 2.

Figure 13.- Continued.

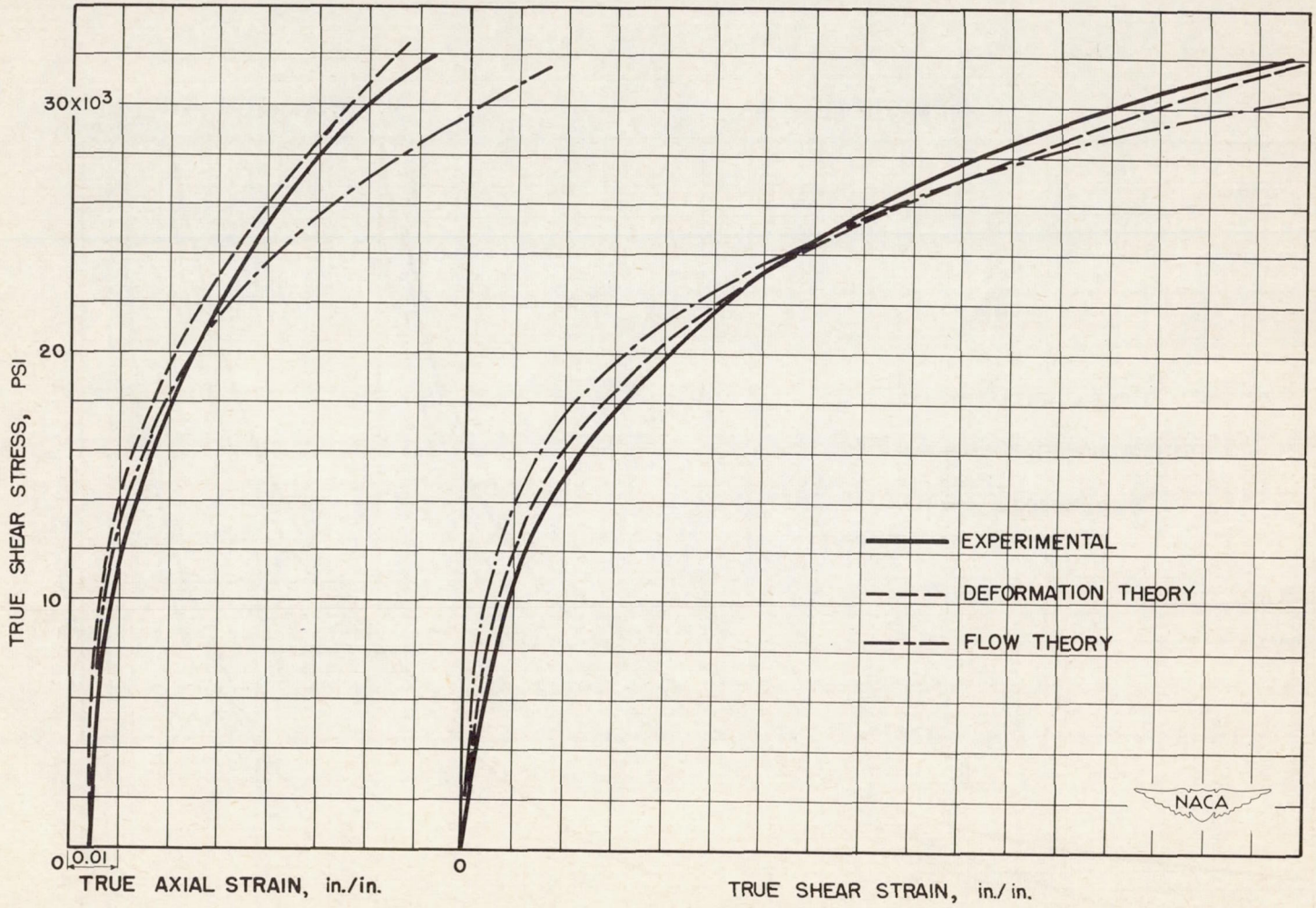

(c) Set A, test 3.

Figure 13.- Continued.

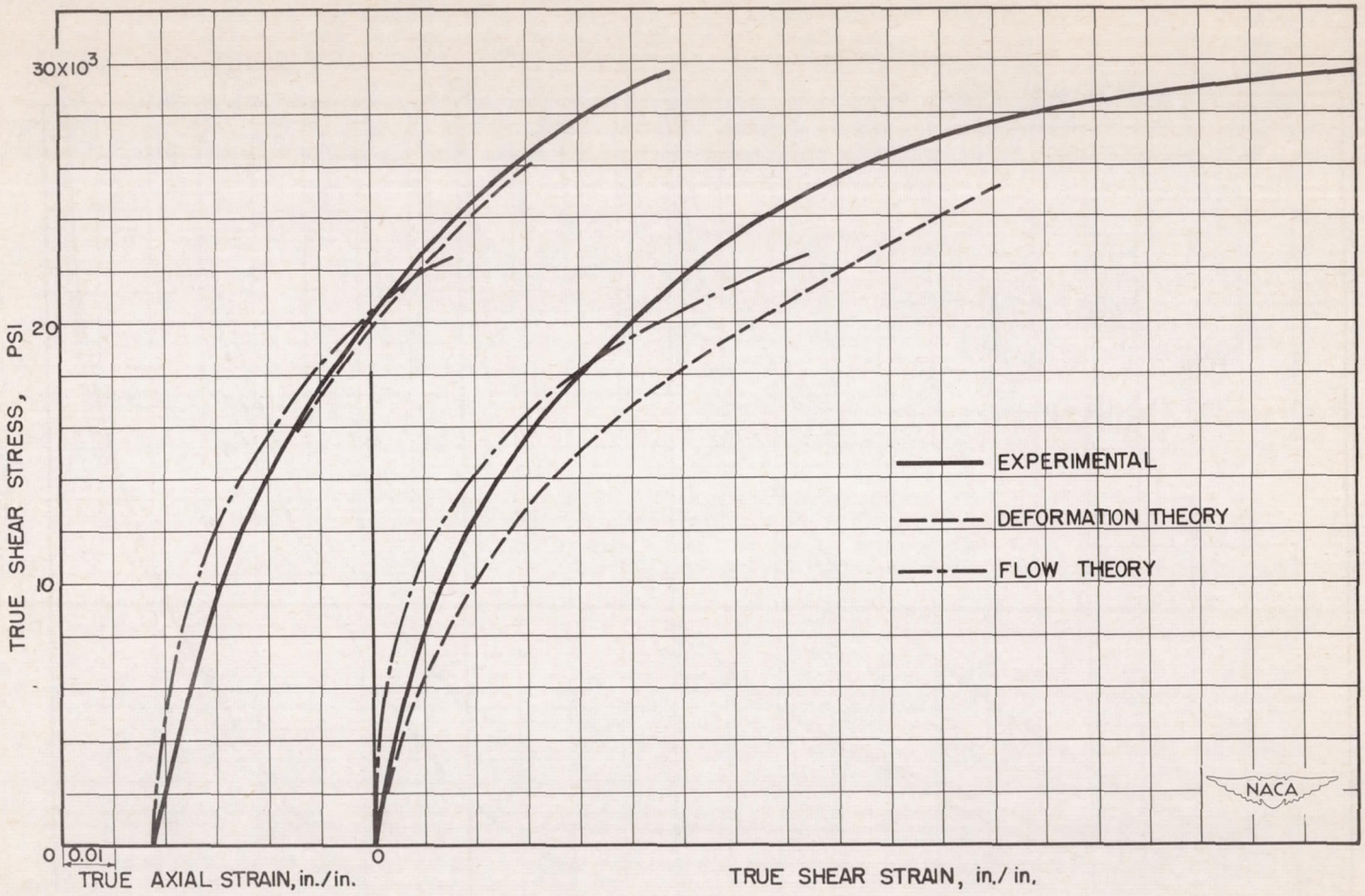

(d) Set A, test 4.

Figure 13.- Continued.

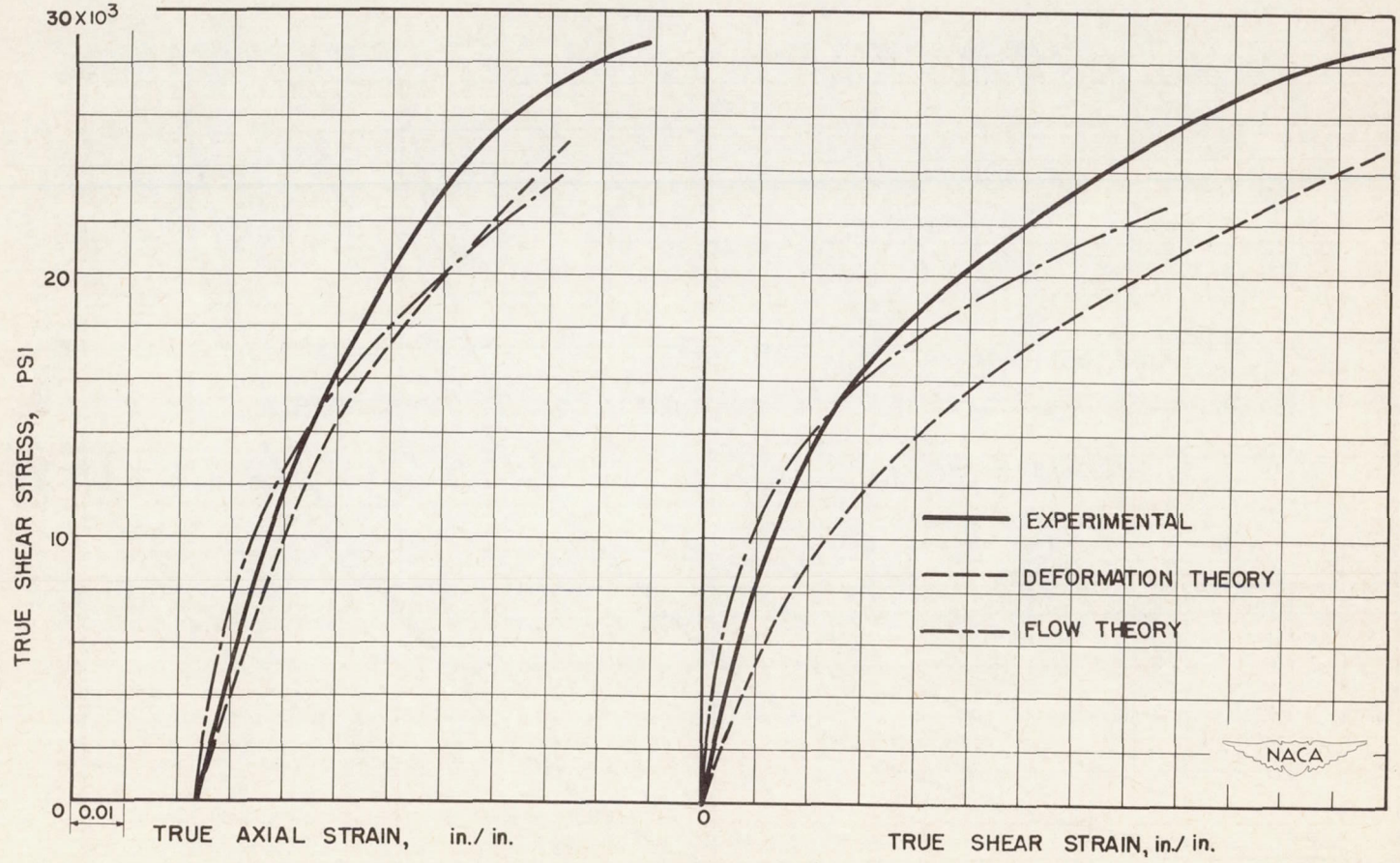

(e) Set A, test 5.

Figure 13.- Concluded.

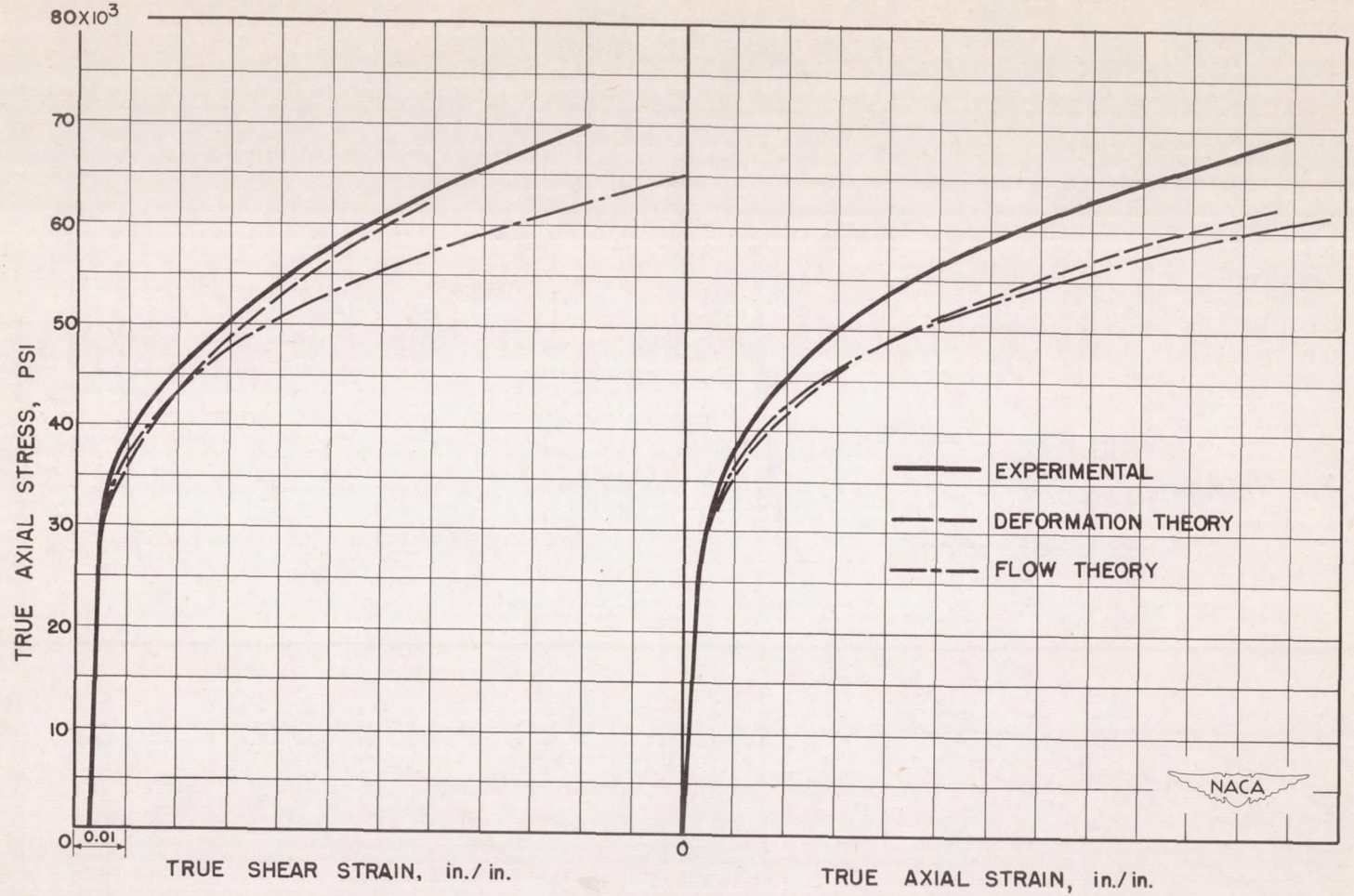

(a) Set B, test 1.

Figure 14.- Comparison of true stress-strain diagrams with plasticity theories for variable-stress-ratio tests.

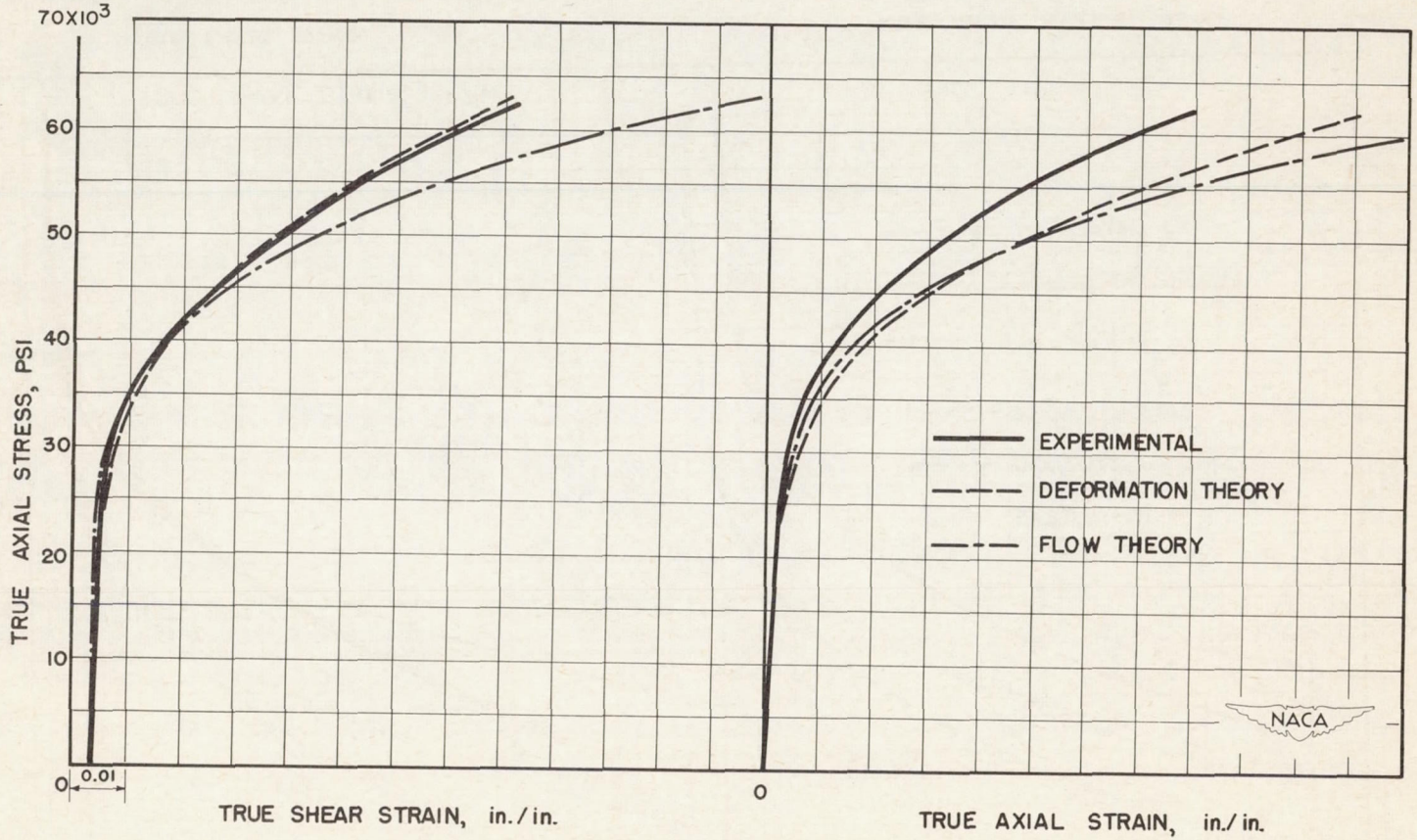

(b) Set B, test 2.

Figure 14.- Continued.

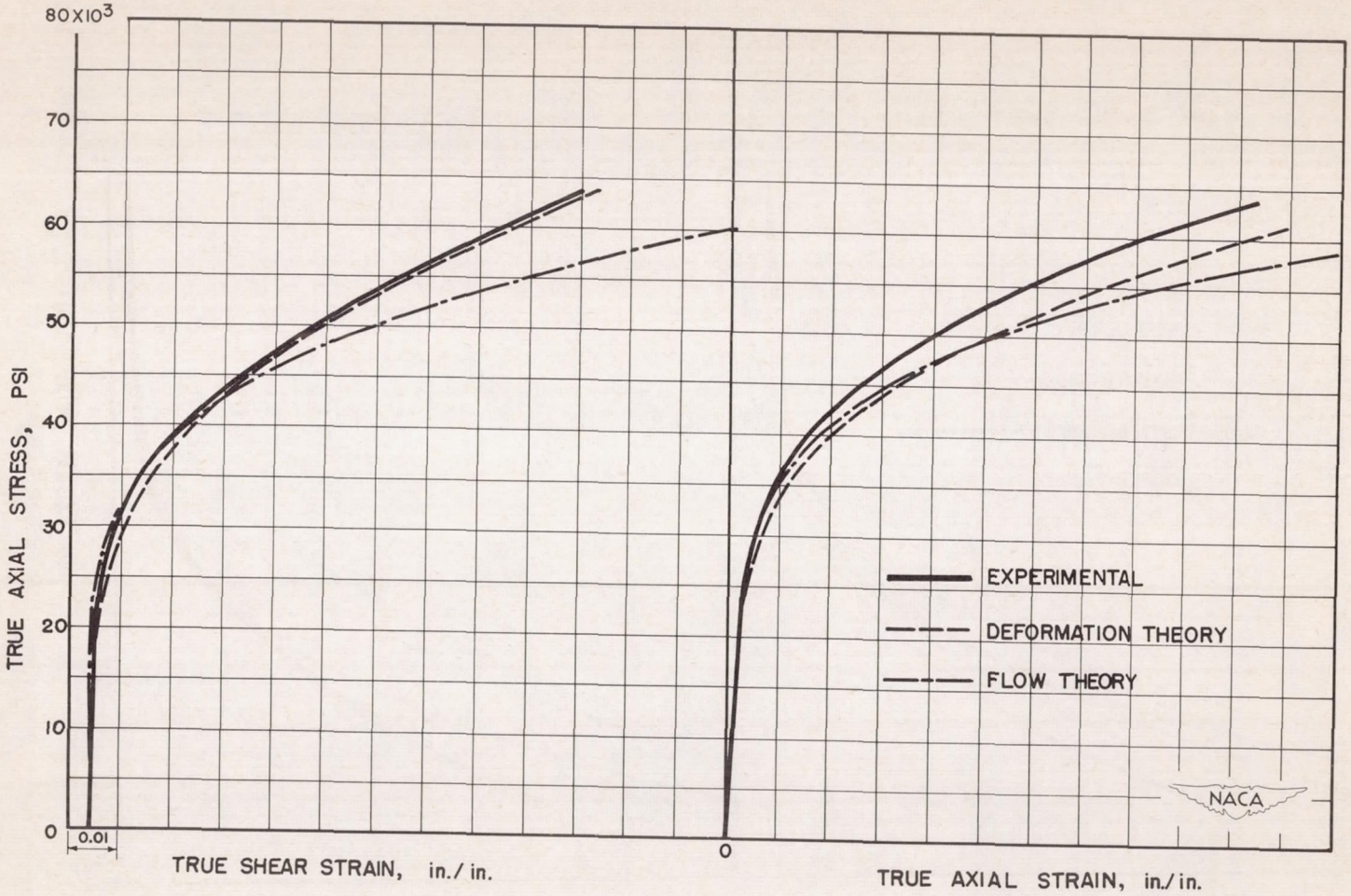

(c) Set B, test 3.

Figure 14.- Continued.

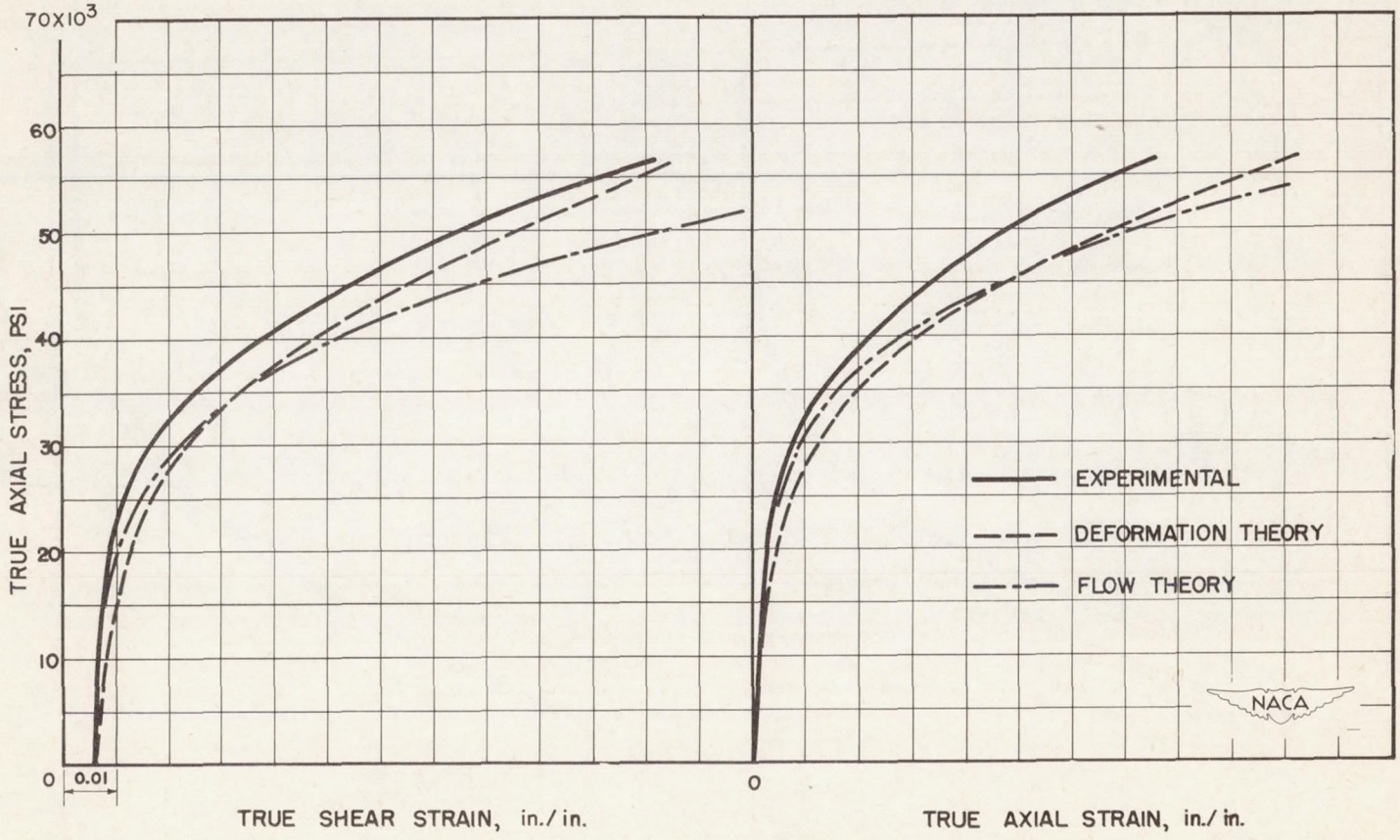

(d) Set B, test 4.

Figure 14.- Continued.

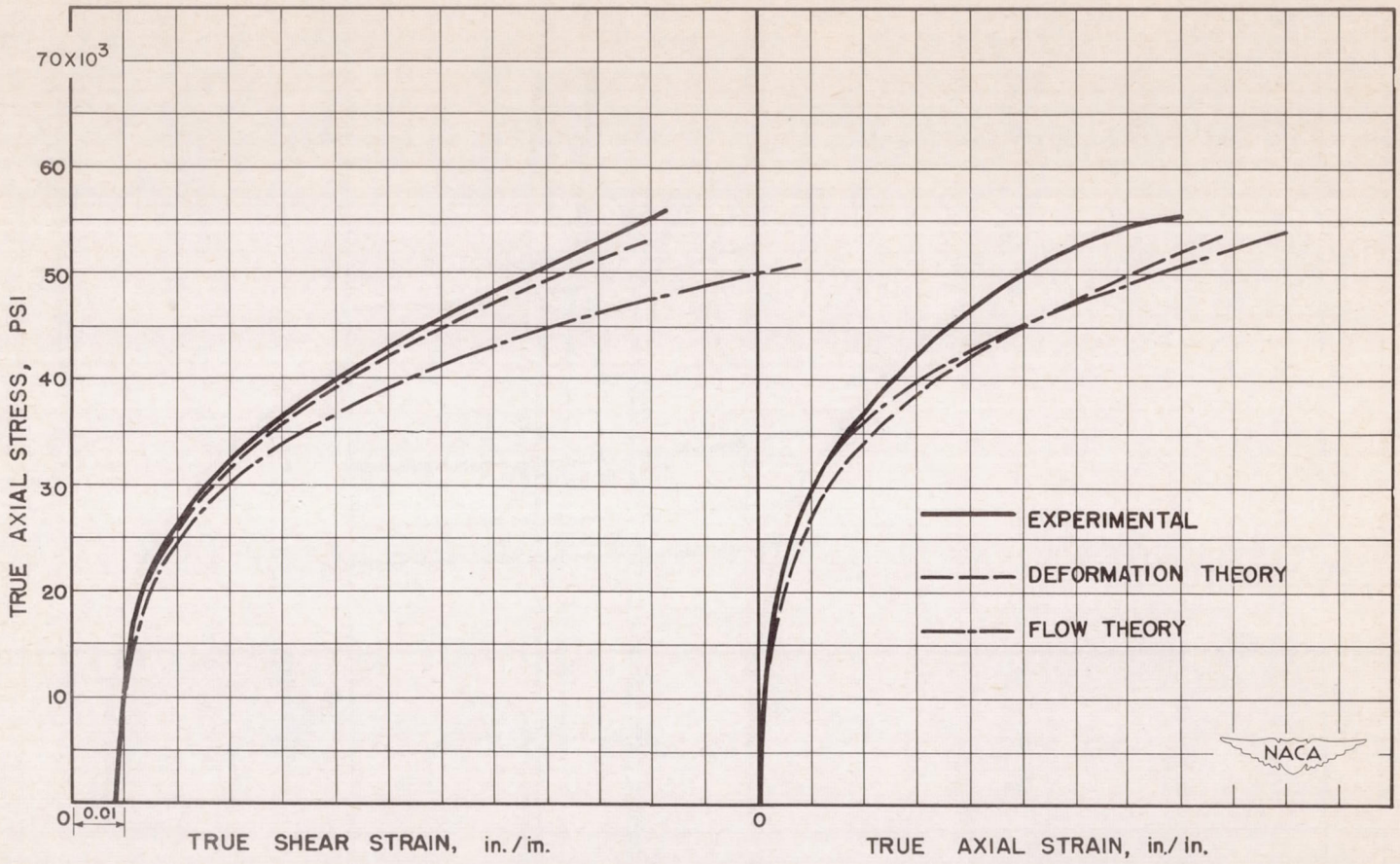

(e) Set B, test 5.

Figure 14.- Concluded.

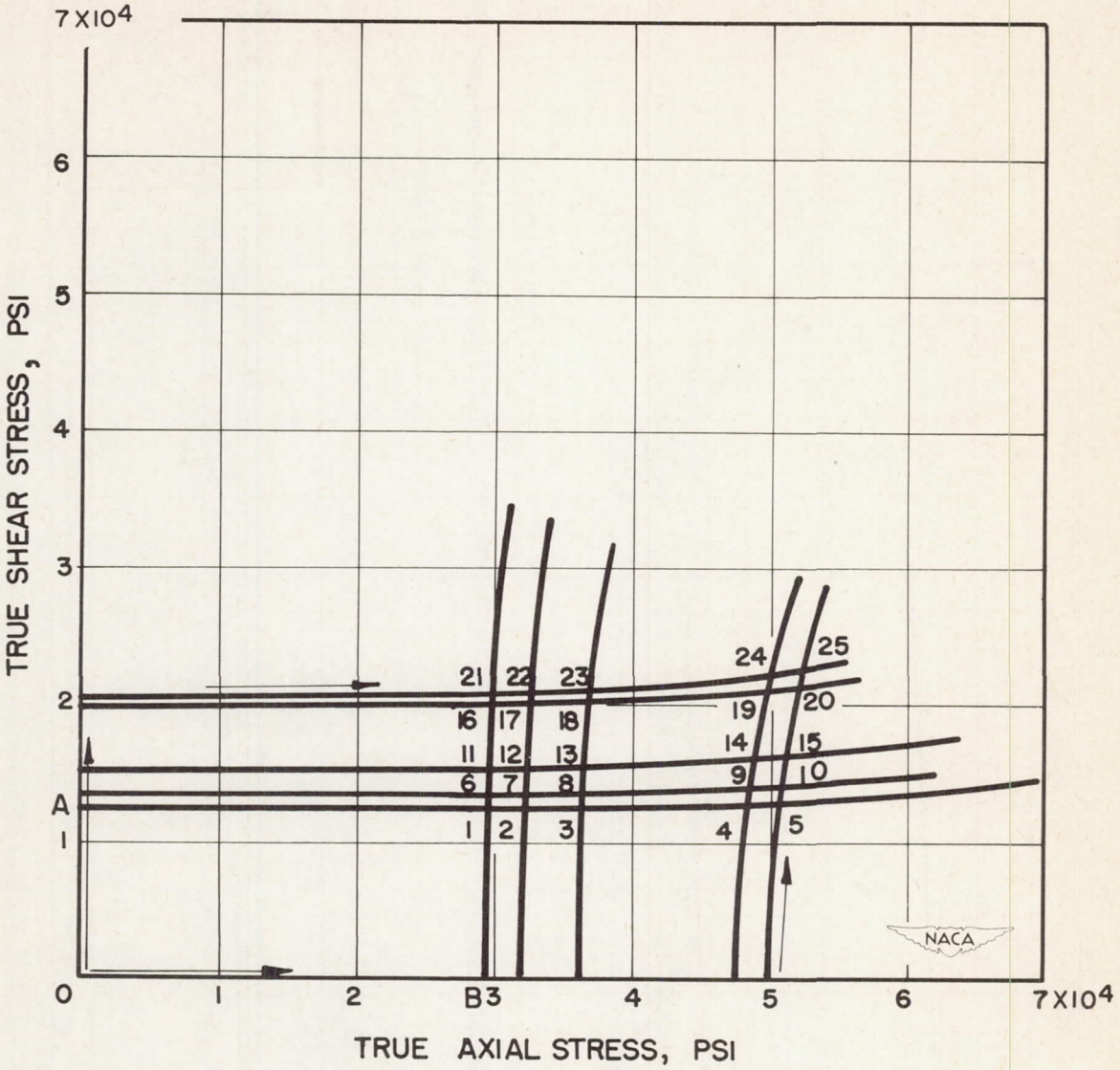

Figure 15.- Loading path for variable-stress-ratio tests.

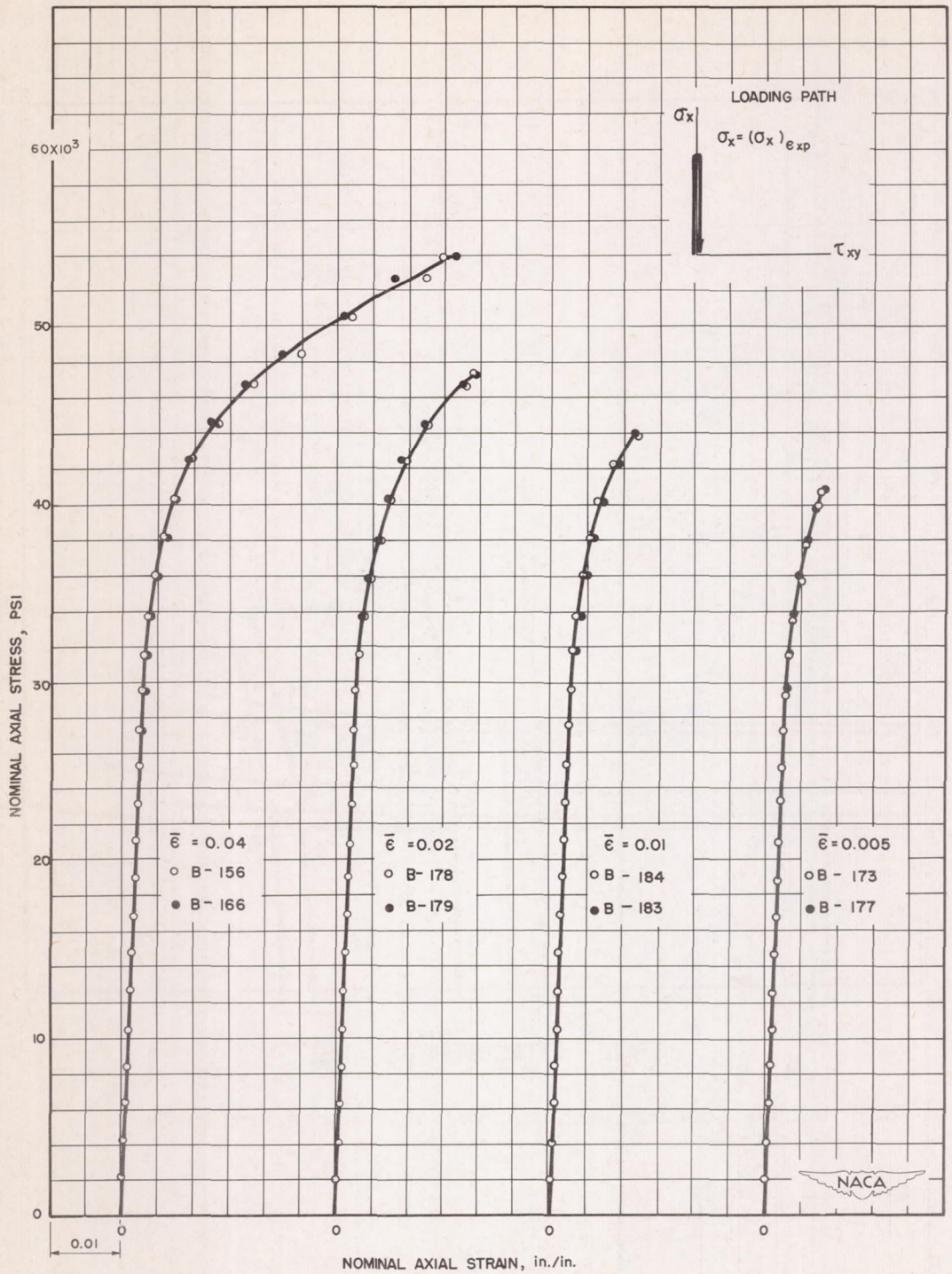

(a) Set C, test 1.

Figure 16.- Nominal stress-strain relations for special test.

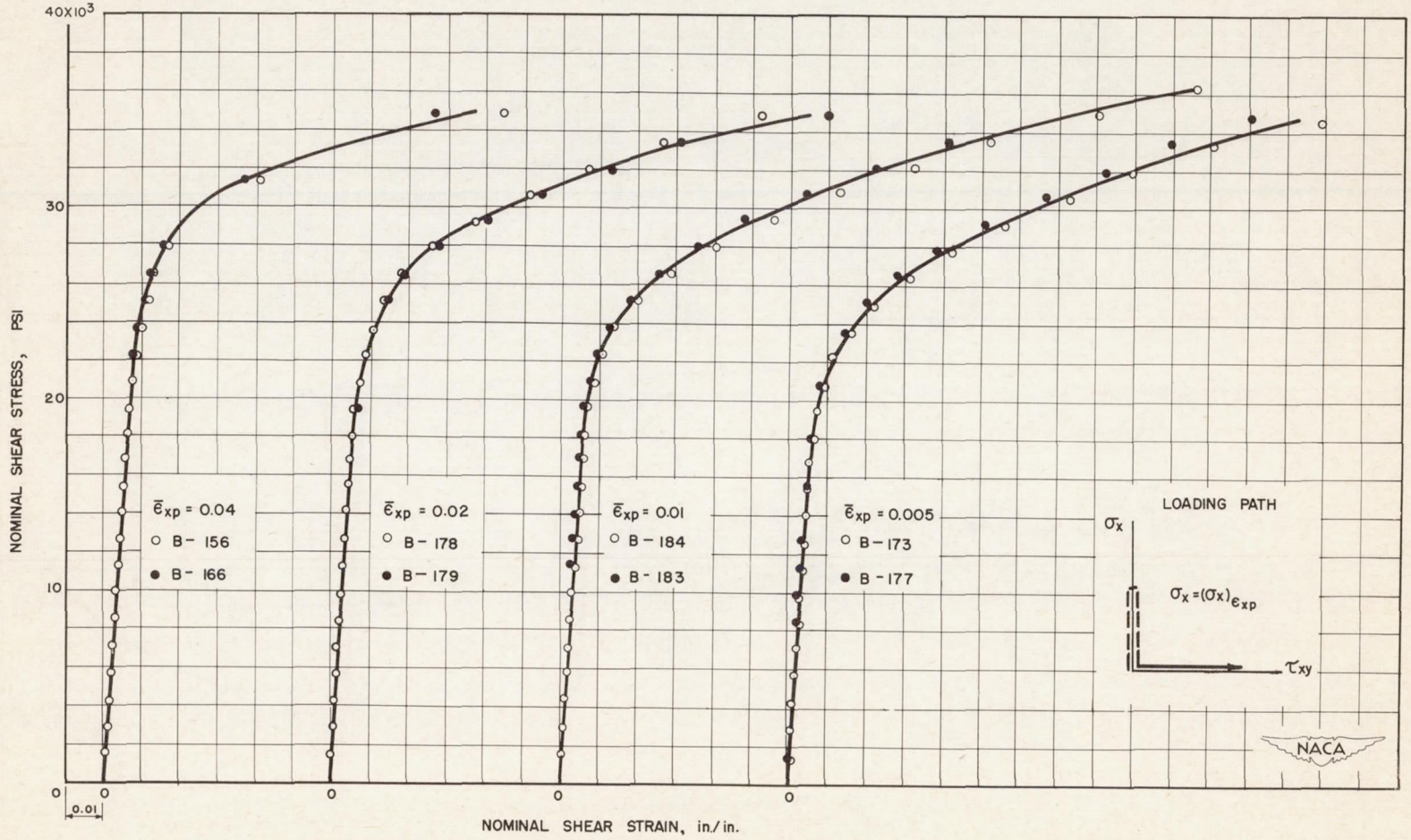

(b) Set C, test 2.

Figure 16.- Concluded.

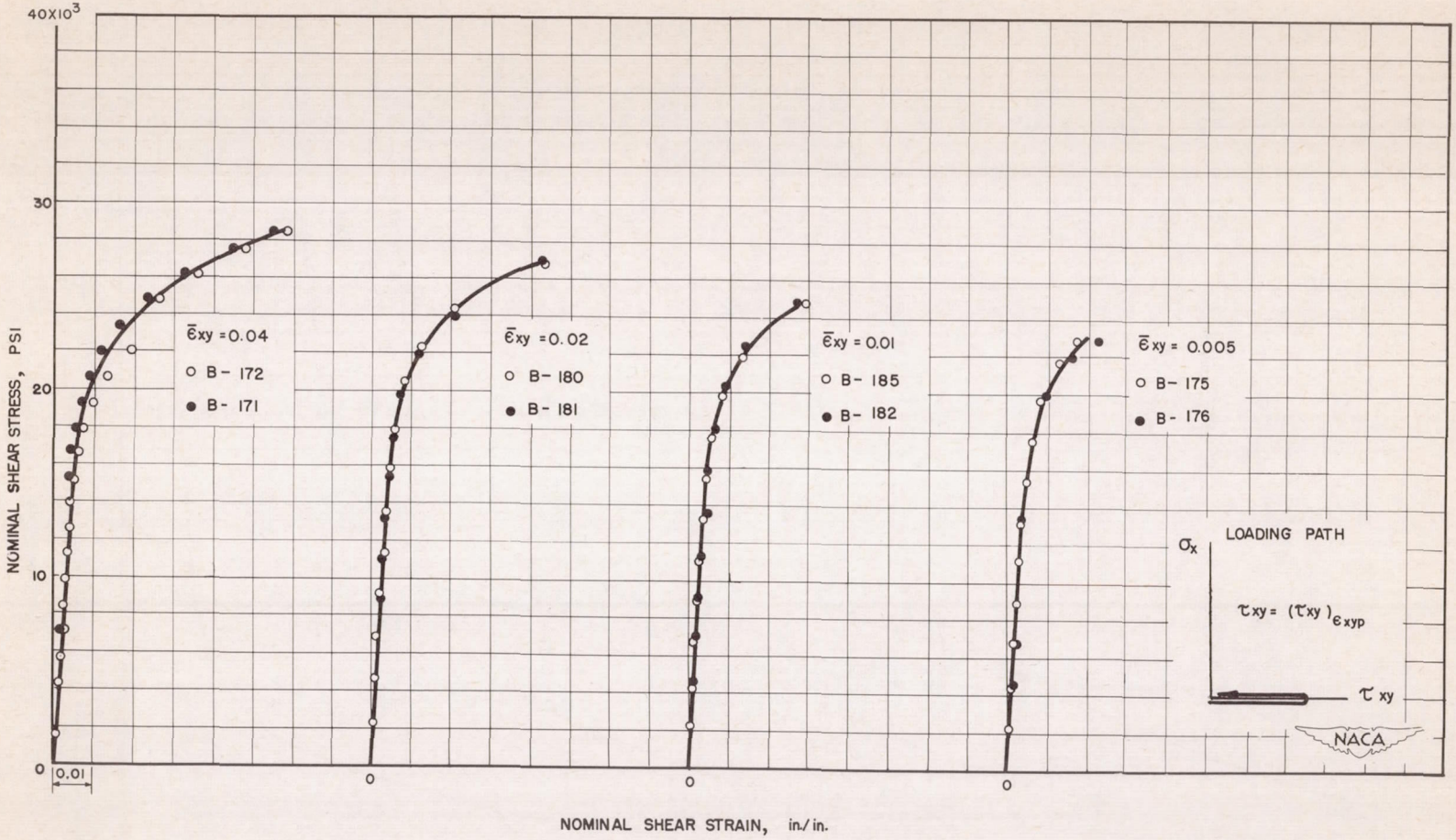

(a) Set D, test 1.

Figure 17.- Nominal stress-strain relations for special test.
F denotes fracture.

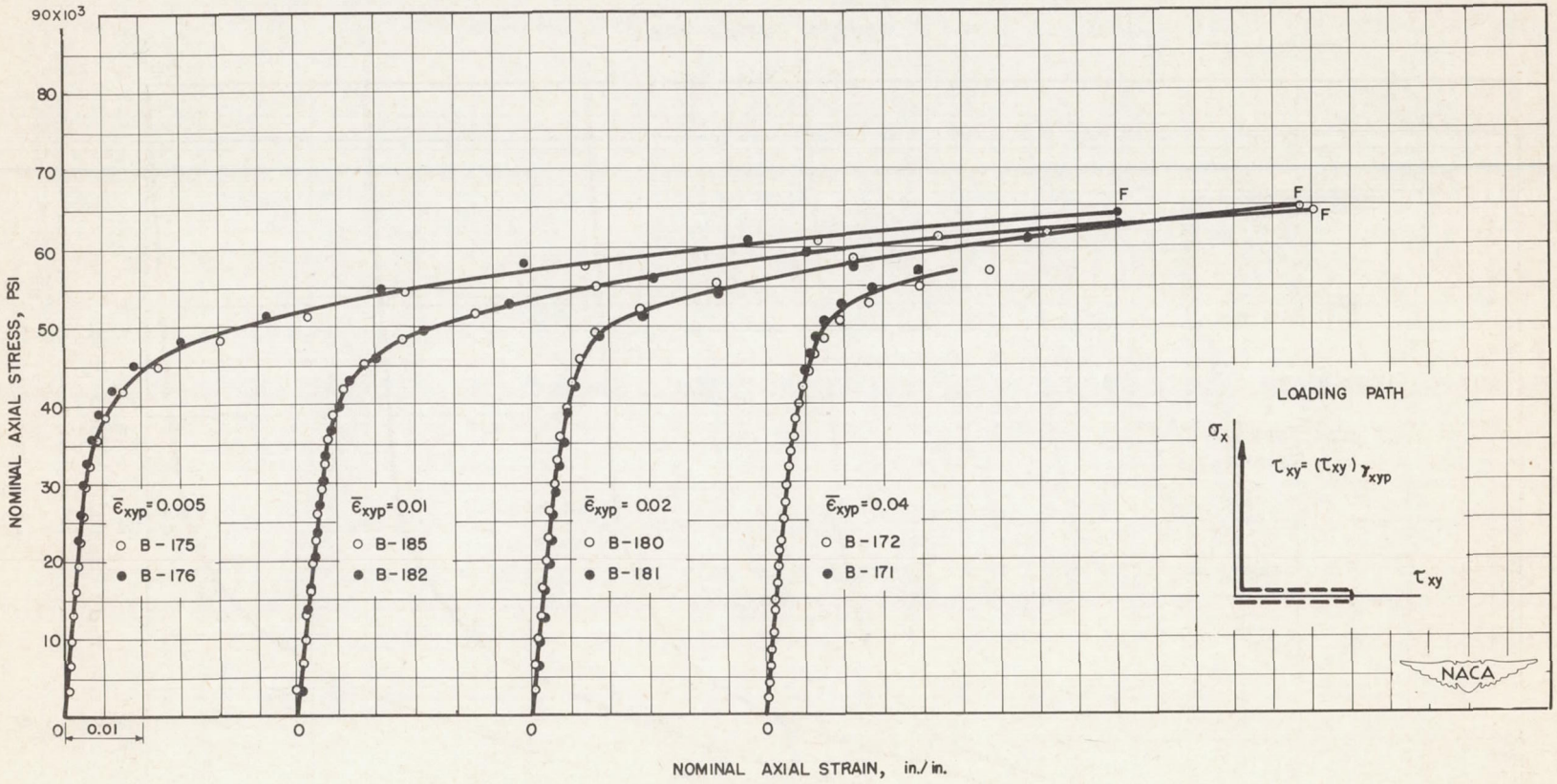

(b) Set D, test 2.

Figure 17.- Concluded.

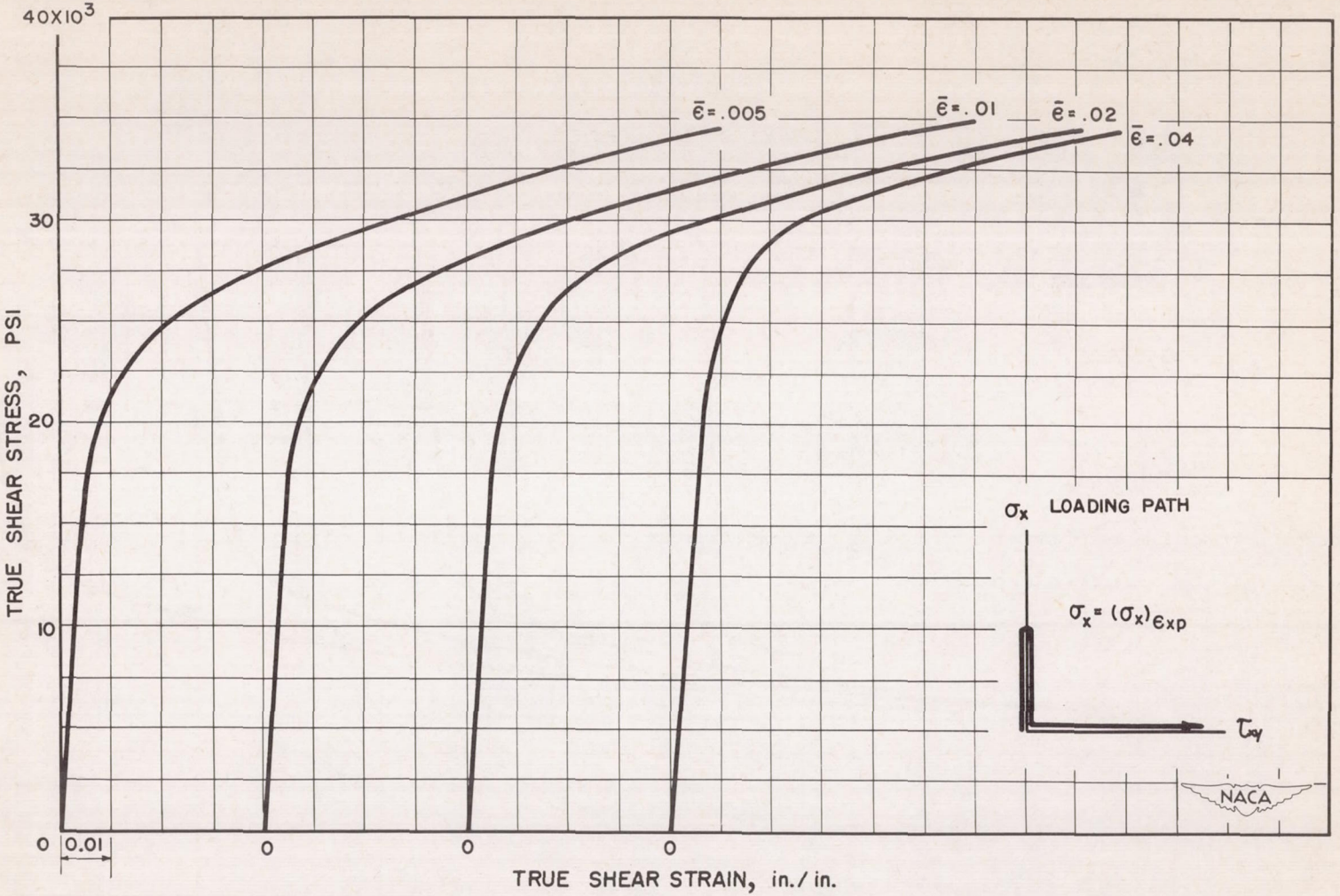

(a) Set C.

Figure 18.- True stress-strain relations for special tests.

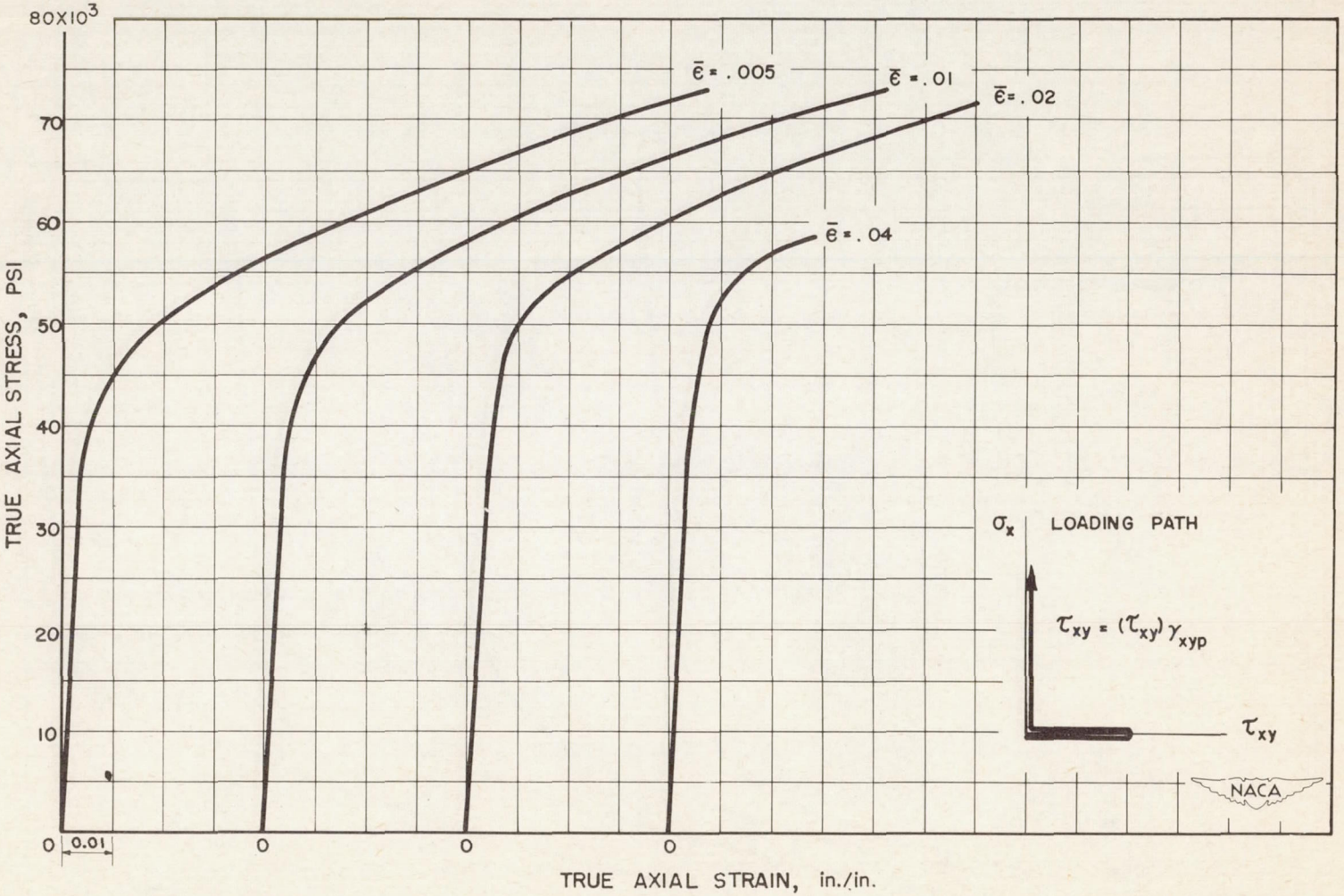

(b) Set D.

Figure 18.- Concluded.

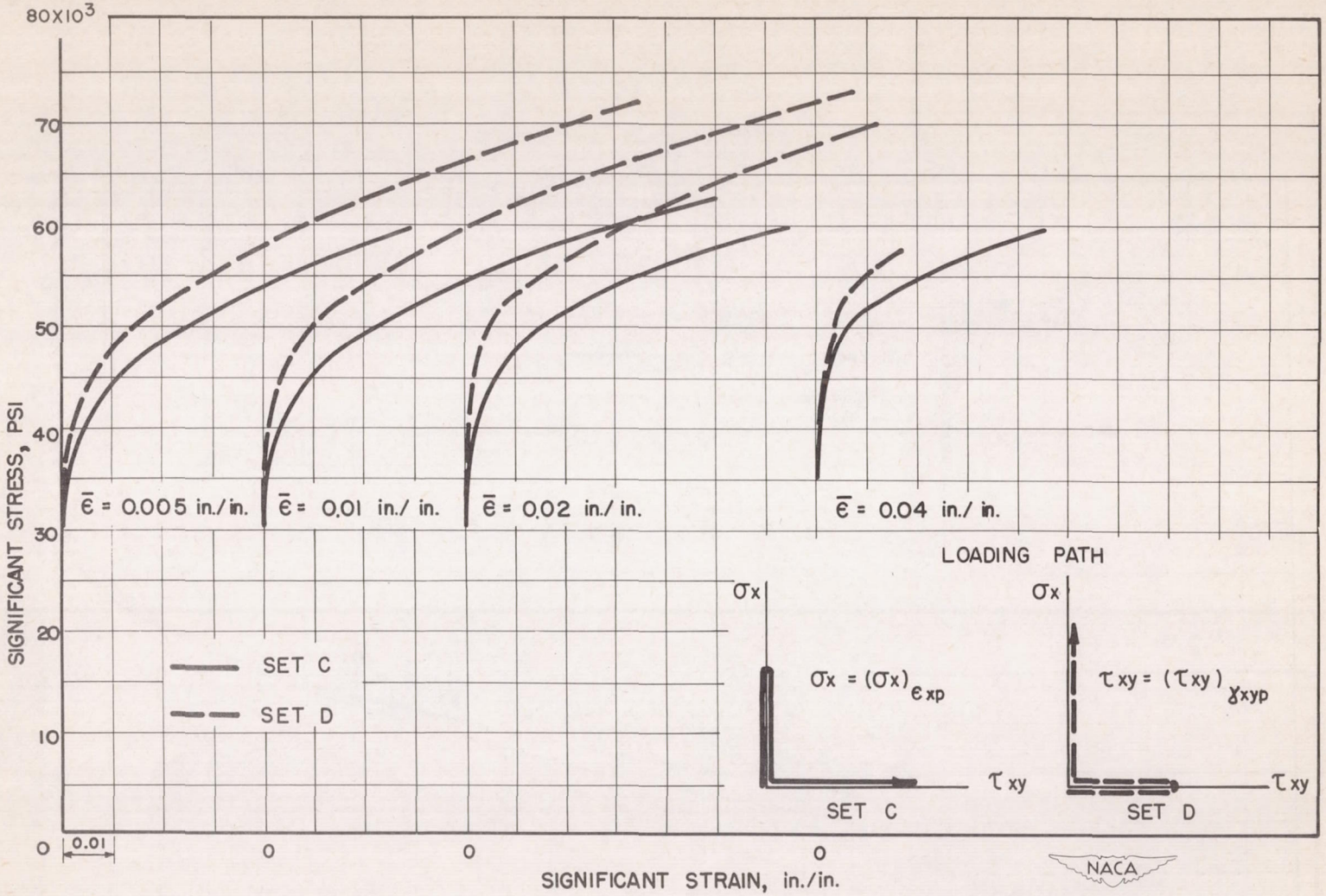

Figure 19.- Comparison of significant stress-strain relations for special tests. Sets C and D.

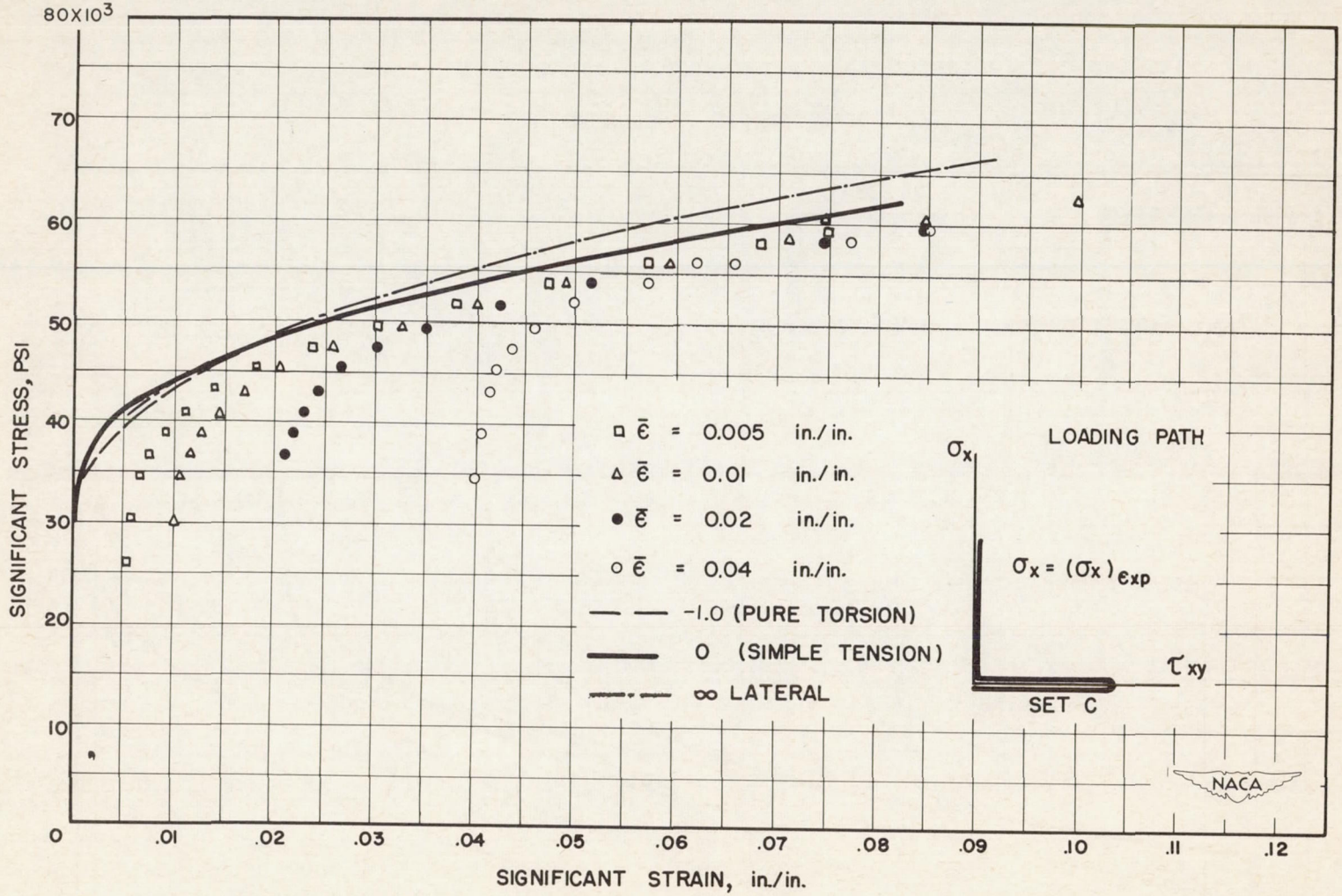

(a) Set C.

Figure 20.- Comparison of significant stress-strain relations for special tests.

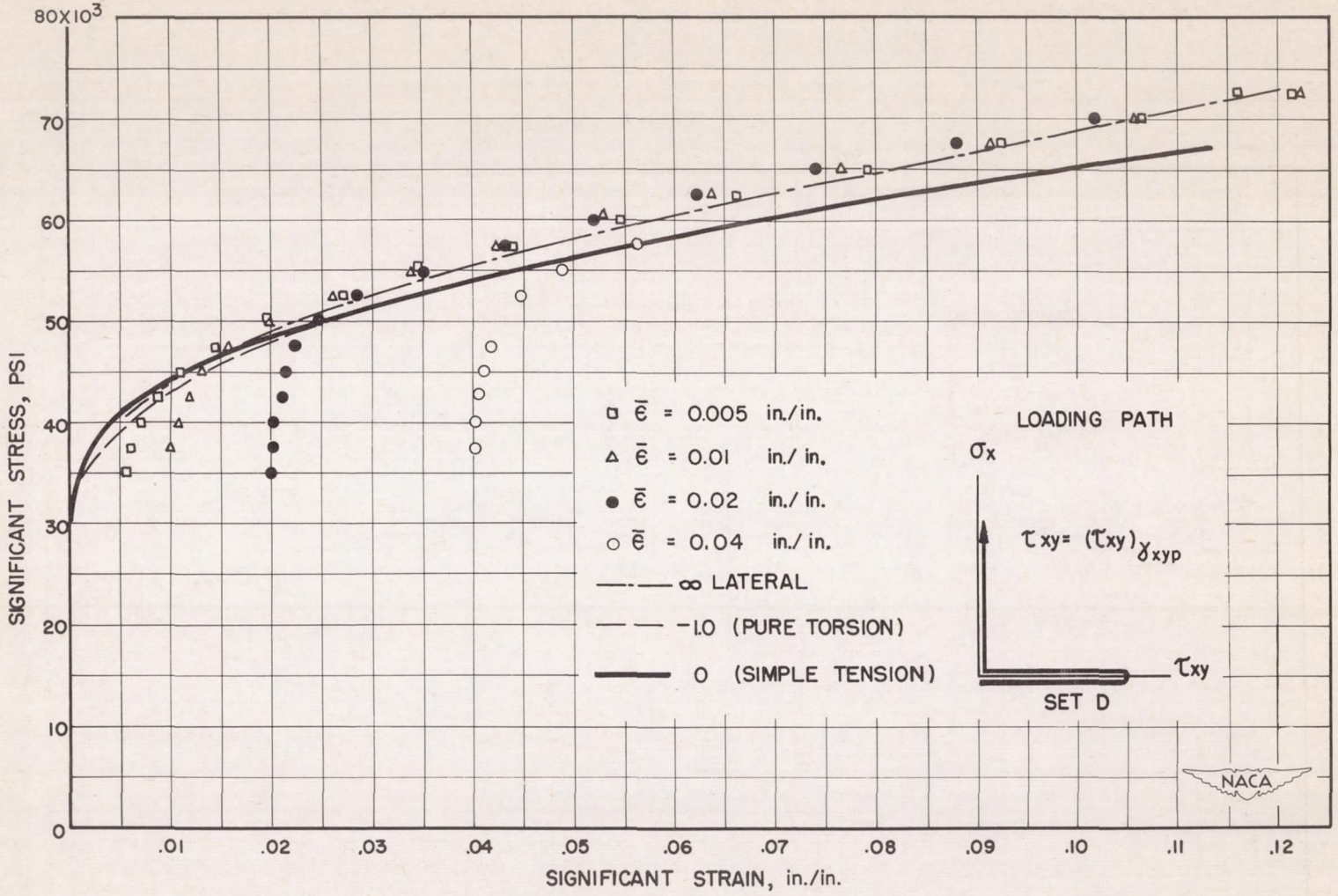

(b) Set D.

Figure 20.- Concluded.

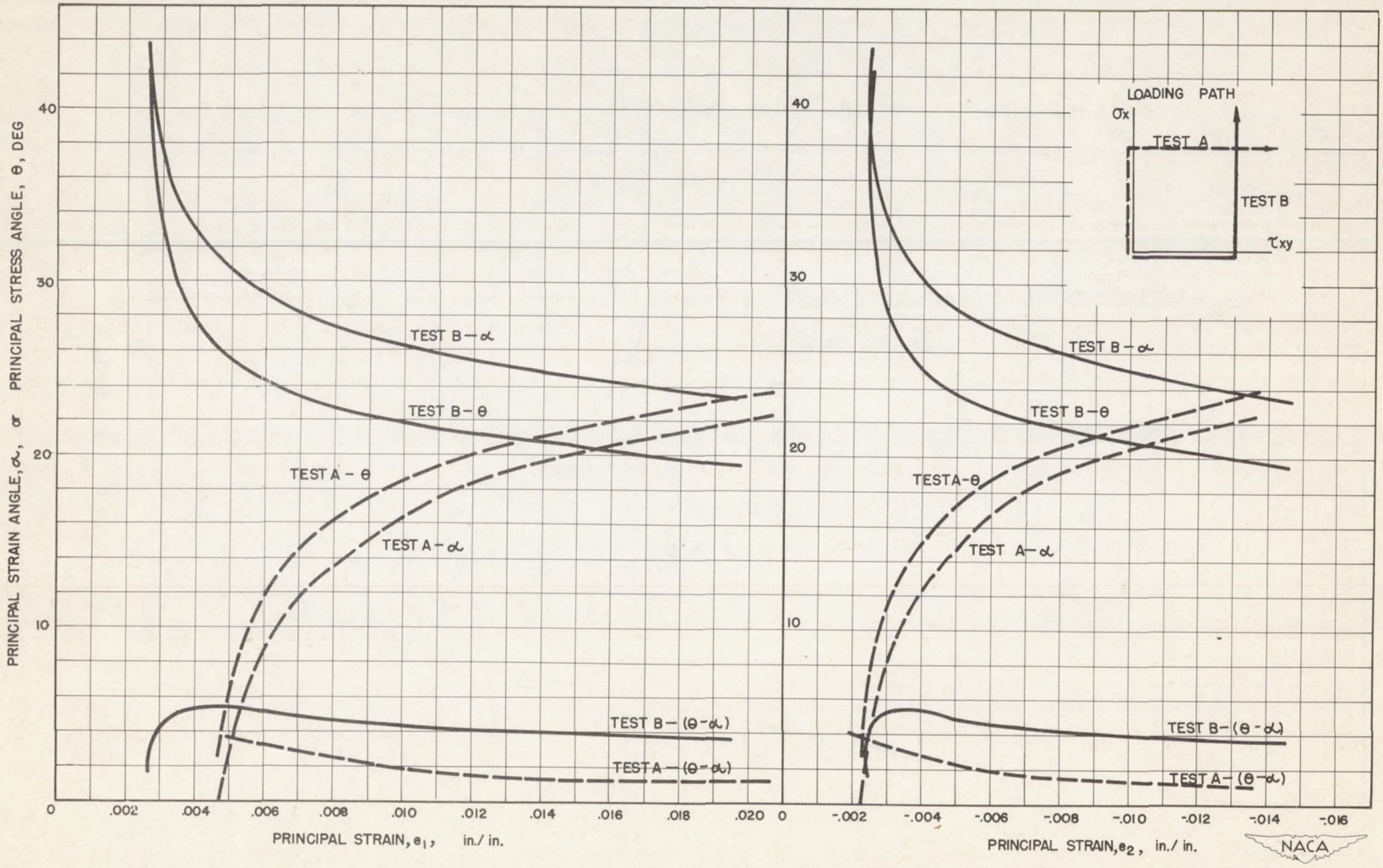

Figure 21.- Comparison of principal strain and stress directions.

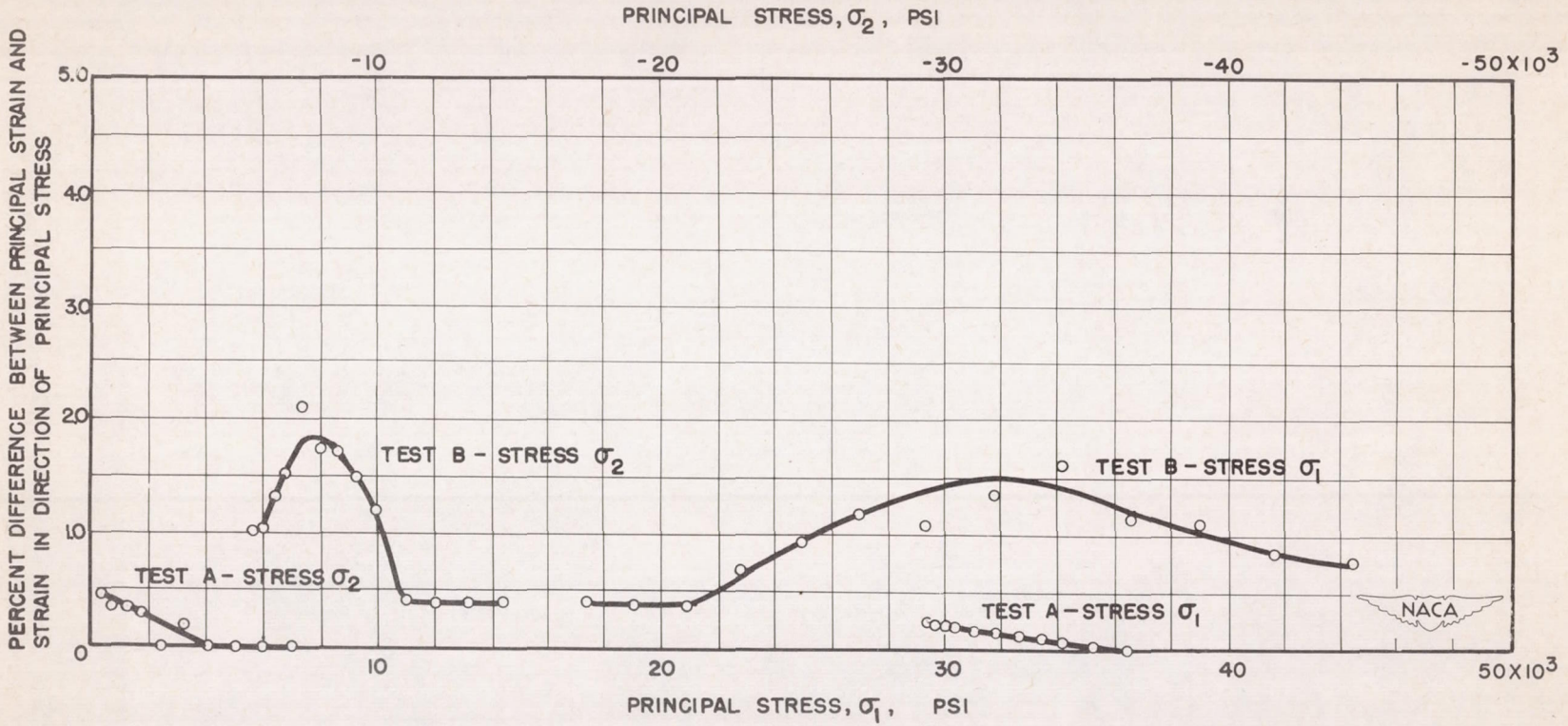

Figure 22.- Difference between principal strain and strain in direction of principal stress.